PART I:

AN ANALYSIS OF REINER'S CENTRIPETAL PUMP

Part II:

A STUDY OF SOME TURBULENT FLOWS USING A MODEL FOR INHOMOGENEOUS TURBULENCE

Thesis by

Shakkottai P. Govindaraju

In Partial Fulfillment of the Requirements

For the Degree of

Doctor of Philosophy

California Institute of Technology

Pasadena, California 91109

1970

(Submitted May 11, 1970)

ACKNOWLEDGEMENT

I appreciate very much the guidance of Dr. P. G. Saffman who suggested the problems and provided advice and direction throughout the course of this work. I thank Mr. A. Vijayaraghavan for several useful discussions.

I appreciate the financial support provided by the Guggenheim Wind Tunnel Fellowship and a Graduate Research Assistantship during the past four years.

Finally, I thank Mrs. Vivian Davies for the excellent typing of the thesis.

ABSTRACT

Part I

A centripetal pump consists of a self-aligning rotor in rotation close to a fixed plane stator. In such an apparatus Reiner observed an excess air pressure in the gap between the discs over ambient and a consequent repulsive force between the discs. Reiner interpreted this repulsive force to be the result of non-Newtonian properties of air. Since this hypothesis is in contradiction with known behavior of air in other similar situations, we try to explain it as due to imperfections of the apparatus used and consider three possibilities: dynamic unbalance of the rotor, instability of the rotor and vibrations of the stator. The results of the analyses show that the third possibility can explain Reiner's observations under some reasonable assumptions. It is concluded that Reiner's hypothesis is unjustified.

Part II

A model for inhomogeneous turbulence, due to Saffman, describes turbulence in terms of two scalar densities governed by nonlinear diffusion equations. Using this model some turbulent flows are studied to assess the value of the model as a basis for analyzing turbulent flows. The specific problems studied include the two-dimensional wake, the two-dimensional jet, the turbulent couette

flow, flow in a channel and the turbulent trailing vortex. Predictions based on the model agree fairly well with experimental results except for the turbulent trailing vortex. Some shortcomings of the model as evident from the application are discussed.

TABLE OF CONTENTS

Part I

TABLE OF CONTENTS (Cont'd)

Part II

PART I

An Analysis of Reiner's Centripetal Pump

1. Introduction.

A 'centripetal pump' consists of two discs—a stator S which is fixed and a rotor R which rotates—with a small air gap between them. Popper and Reiner (1956) demonstrated that when the gap between R and S is very small (of the order of a few microns) the air pressure in the gap at the center of the discs is higher than ambient by as much as 50 cms of water. This might be appropriately called the 'Reiner effect'. Since an analysis based on Newtonian behavior of air and perfectly parallel discs (Stewartson's solution) predicts a small suction at the center of the discs, Reiner suggested that the Reiner effect is due to viscoelastic properties of air.

Velocity gradients comparable to those in Reiner's experiments occur in boundary layers. Analyses of boundary layers based on Newtonian behavior of air yield results in agreement with experiments (Schlichting 1954). Also, calculations (Taylor and Saffman 1957) show that non-Newtonian properties of air are too small to account for Reiner's observations. So, Taylor and Saffman tried to explain the Reiner effect as due to imperfections of the apparatus used. They considered two possible imperfections: (a) a small tilt of the stator (b) small normal oscillations of the rotor relative to the stator. They made some estimates of pressure rise at the center of the discs and these roughly agreed with Reiner's observations.

In order to reduce the imperfections, if any, of the types considered by Taylor and Saffman, Reiner built the apparatus shown in Fig. 1. Here the rotor R is centered by a ball and is driven by a pin which is free to move along a pair of slots in the rotor. Thus

the rotor is free to align itself parallel to the stator. Also, axial motion of the drive shaft, if any, is not transmitted to the rotor. Thus, it is seen that the weight of rotor tends to bring the two discs together. Reiner found that, when in rotation, the rotor did not contact the stator but floated on a thin film of air (a few microns thick). Although, under similar conditions, the mean pressure between the two discs with the new apparatus was about a tenth of that with the old apparatus, Reiner still considered the effect as due to viscoelastic properties of air and made no effort to explain the difference between the two sets of results. If the Reiner effect were due to imperfections of the apparatus, one could explain such a difference as due to differences in the imperfections of the two machines. Thus, the new results seem to reinforce the hypothesis of Taylor and Saffman.

In what follows we try to explain Reiner's observations made on the new apparatus on the basis of Newtonian behavior of air and consider the following possibilities.

(1) The rotor is not in dynamic balance so that the rotor is acted on by a moment due to centrifugal forces. The rotor tilts due to this moment and results in a situation similar to the one considered by Taylor and Saffman.

(2) The position of the rotor when it is parallel to the stator is unstable so that the rotor executes self-excited oscillations.

(3) There exist vibrations of the stator excited by imperfections in the drive system.

2. Analysis.

2.1 Effect of Rotor Unbalance.

In Reiner's apparatus of Fig. 1, the center of gravity of the rotor is above the center of the locating ball by about 1.5 mm. Thus if, due to errors in machining, the center of gravity of the rotor does not fall on the axis of rotation, the rotor, during rotation, will experience a moment due to centrifugal acceleration. Such a moment will be resisted by hydrodynamic forces in the airfilm if the rotor tilts an appropriate amount. The tilted rotor also produces lift which can resist the weight of the rotor.

To see whether the above possibility can provide a reasonable explanation for Reiner's observations, we analyze the steady motion of a rotor whose axis makes a small angle with the axis of rotation.

The pressure p' which is taken as a function of polar coordinates r', θ' and time t' is governed by the equation (Saffman 1957)

$$\frac{\partial}{\partial r'}\left(\frac{r'h'^3\rho'}{\mu}\cdot\frac{\partial p'}{\partial r'}\right)+\frac{\partial}{\partial \theta'}\left(\frac{\rho'h'^3}{\mu r'}\cdot\frac{\partial p'}{\partial \theta'}\right)=6\Omega\frac{\partial}{\partial \theta'}(\rho'r'h')+12\frac{\partial}{\partial t'}(\rho'r'h') \quad (2.1)$$

where h', the thickness of the air film between the rotor and the stator, is a function of r', θ' and t'. ρ', the density of air, can be taken as proportional to pressure since the flow, under the conditions we are considering, is known to be very nearly isothermal (Salbu 1964).

Introducing new variables:

$$r = \frac{r'}{a}\ ,\quad t = \Omega t'\ ,\quad p = \frac{p'-p_0}{p_0}\ ,$$

$$h = \frac{h'}{h_0}\ ,\quad \rho = \rho_0(1+p)\ ,\quad \theta = \theta' - \int_0^{t'} \frac{d\phi}{d\tau}(\tau)\, d\tau \qquad (2.2)$$

(2.1) can be written, in dimensionless form, as:

$$\frac{\partial}{\partial r}\left\{rh^3(1+p)\frac{\partial p}{\partial r}\right\} + \frac{\partial}{\partial \theta}\left\{\frac{h^3(1+p)}{r}\cdot\frac{\partial p}{\partial \theta}\right\} = \lambda^* r \frac{\partial}{\partial \theta}\{h(1+p)\} + 2\lambda r \frac{\partial}{\partial t}\{h(1+p)\} \qquad (2.3)$$

where

$$\lambda = \frac{6\Omega\mu a^2}{p_0 h_0^2}\ ,\quad \lambda^* = \lambda(1-2\dot{\phi})\ ,\quad \dot{\phi} = \frac{d\phi}{dt} = \frac{1}{\Omega}\frac{d\phi}{dt'} \qquad (2.4)$$

ϕ is the angular position of the radius of greatest rotor inclination with respect to a fixed direction ox' as in Fig. 2. Thus $\frac{d\phi}{dt'}$ is the speed of nutation of the rotor.

For steady rotation, $\frac{d\phi}{dt} = 1$ and (2.3) reduces to

$$\frac{\partial}{\partial r}\left(rh^3(1+p)\frac{\partial p}{\partial r}\right) + \frac{\partial}{\partial \theta}\left(\frac{h^3}{r}(1+p)\frac{\partial p}{\partial \theta}\right) = \lambda^* r \frac{\partial}{\partial \theta}\{h(1+p)\} \qquad (2.5)$$

with

$$\lambda^* = \lambda(1-2\dot{\phi}) = -\lambda\ .$$

For any specified distribution of h, one has to solve (2.5) subject to the boundary condition $p = 0$ at $r = 1$. For a small inclination of the rotor relative to the stator, one can take

$$h = 1 + e\,r\cos\theta \tag{2.6}$$

where eh_0/a is the angle between the plates.

Eqn. (2.5) with h given by Eqn. (2.6) can be solved for small values of e (i.e. $e << 1$) by seeking a solution of the form

$$p = p_1 e + p_2 e^2 + p_3 e^3 + \cdots \tag{2.7}$$

Such a solution was obtained by Taylor and Saffman for the case when λ^* of Eqn. (2.5) was equal to λ. For the present case with $\lambda^* = -\lambda$, we can easily obtain p_1 as

$$p_1 = A(r)\cos\theta + B(r)\sin\theta \tag{2.8}$$

where

$$A - iB = C(r) = \frac{J_1(\sqrt{i\lambda}\cdot r)}{J_1(\sqrt{i\lambda})} - r \tag{2.9}$$

and the mean value of p, defined by $\bar{p} = \frac{1}{2\pi}\int_0^{2\pi} p\,d\theta$, is

$$\bar{p} = \bar{p}_1 e + \bar{p}_2 e^2 + \bar{p}_3 e^3 + O(e^4) \tag{2.10}$$

It is found that $\bar{p}_1 = \bar{p}_3 = 0$ and

$$\bar{p}_2 = \frac{3}{2}\cdot\int_r^1 r\,\frac{dA}{dr}\cdot dr - \tfrac{1}{4}(A^2 + B^2) \tag{2.11}$$

The resultant hydrodynamic forces on the rotor are

(a) A force along oz which is resisted by the normal component of rotor weight.

(b) Small lateral forces along oy and oz which are resisted by the centering ball.

(c) A torque about oz which is resisted by the drive shaft.

(d) Moments about the ox and oy axes which are resisted by the moments due to centrifugal forces and that due to gravity.

We calculate (a) and (d) only, as (b) and (c) are not relevant. The force along oz is

$$L = \int_0^1 \bar{p}\, 2\pi r\, dr\, p_0 a^2$$

i.e.
$$L = 2\pi p_0 a^2 e^2 \int_0^1 \bar{p}_2\, r\, dr + O(e^4) \qquad (2.12)$$

where $\bar{p}_2$ is given by Eqn. (2.11) It is not possible to evaluate L explicitly except for values of λ small compared with 16, when A(r) and B(r) can be expanded as power series in λ. Using such an expansion one finds that

$$\bar{p}_2 = \frac{e^2\lambda^2}{2^8}\left(\tfrac{2}{3}r^6 - \frac{5}{2}r^4 + r^2 + \frac{5}{6}\right) + O(\lambda^4) \qquad (2.13)$$

using this

$$L = \frac{\pi p_0 a^2 e^2 \lambda^2}{3 \times 2^7} + O(\lambda^4 e^2\ , e^4) \qquad (2.14)$$

The moments about the ox and oy axes, M_x and M_y, are given by

$$M_x = p_0 a^3 \int_0^{2\pi} \int_0^1 p\, r^2 \sin\theta \cdot dr\, d\theta$$

$$= p\, a^3 e \int_0^{2\pi} \int_0^1 p_1 r^2 \sin\theta \cdot dr\, d\theta + O(e^2)$$

$$= p\, a^3 e \int_0^{\pi} \int_0^1 (A(r)\cos\theta + B(r)\sin\theta) \sin\theta\, r^2\, dr\, d\theta + O(e^2)$$

$$= p_0 \pi a^3 e \int_0^1 B(r)\, r^2 \cdot dr + O(e^2) \qquad (2.15)$$

Similarly,

$$M_y = -p_0 \pi a^3 e \int_0^1 A(r)\, r^2\, dr + O(e^2) \qquad (2.16)$$

From (2.15) and (2.16) we have

$$M_y + iM_x = -p_0 \pi a^3 e \int_0^1 \{A(r) - iB(r)\} r^2\, dr + O(e^2)$$

$$= -p_0 \pi a^3 e \int_0^1 C(r)\, r^2\, dr + O(e^2)$$

Then using Eqn. (2.9), we have

$$M_y + iM_x = -p_0 \pi a^3 e \int_0^1 \left\{ \frac{J_1(\sqrt{i\lambda}\, r)}{J_1(\sqrt{i\lambda})} - r \right\} r^2\, dr + O(e^2)$$

$$= -p_0 \pi a^3 e \left\{ \frac{J_2(\sqrt{i\lambda})}{\sqrt{i\lambda}\ J_1(\sqrt{i\lambda})} - \tfrac{1}{4} \right\} + O(e^2)$$

$$= -\frac{p_0 \pi a^3 e}{4} \frac{J_3(\sqrt{i\lambda})}{J_1(\sqrt{i\lambda})} + O(e^2) \qquad (2.17)$$

For small values of λ, we expand $M_y + iM_x$ as a series in λ to obtain

$$M_y + iM_x = - p_0 \pi a^3 e \left\{ \frac{i\lambda}{96} - \frac{\lambda^2}{1536} + O(\lambda^3) \right\} + O(e^2) \tag{2.18}$$

From (2.18) we can obtain M_y and M_x separately as

$$M_y = \frac{p_0 \pi a^3 e \lambda^2}{1536} + O(e^2, \lambda^4 e)$$

$$M_x = - \frac{p_0 \pi a^3 e \lambda}{96} + O(e^2, \lambda^3 e) \tag{2.19}$$

Now, we proceed to calculate the forces and moments due to gravity and centrifugal acceleration. We choose a coordinate system oxyz with the origin at the center of the stator such that the projection of the radius of maximum rotor inclination falls along ox as in Fig. 2. Let z_0 be the z coordinate of the center of the ball. Let x_g, y_g, z_g be the coordinates of the center of gravity of the rotor. The moments on the rotor due to the centrifugal forces and gravity can be written as

$$M_x' = -\Omega^2 \int (y_g + y)(z_g - z_0 + z)\, dm - mgy_g$$

where x,y,z are the coordinates of an elemental mass dm. Expanding the integral in the above, we have

$$M_x' = -\Omega^2 mgy_g(z_g - z_0) - mgy_g - \Omega^2 \int yz\, dm .$$

If we idealize the rotor to be a thin disc and further assume that the angle of inclination of the disc, $\frac{eh_0}{a}$ to be small, we have $z = -\frac{eh_0}{a}x$ and thus

$$M_x' = -\Omega^2 m y_g (z_g - z_0) - mg y_g - \frac{\Omega^2 eh_0}{a}\int xy\, dm$$

$$= -\Omega^2 m y_g (z_g - z_0) - mg y_g \qquad (2.20)$$

Similarly, the moment about oy is

$$M_y' = \Omega^2 m x_g (z_g - z_0) + mg x_g + \frac{\Omega^2 eh_0}{a}\int x^2\, dm$$

$$= m\Omega^2 x_g (z_g - z_0) + mg x_g - \frac{m\Omega^2 \alpha a^2}{4} \qquad (2.21)$$

For steady motion $M_y = M_y'$, $M_x = M_x'$ and $L = W$, the force tending to bring the discs together (i.e. = W, the weight of rotor plus the spring load). These conditions, on using (2.12), (2.17), (2.20) and (2.21) give

$$-\frac{p_0 \pi a^3 e}{4} R\left[\frac{J_3(\sqrt{i\lambda})}{J_1(\sqrt{i\lambda})}\right] = m\Omega^2 x_g (z_g - z_0) + mg x_g - \frac{m\Omega^2 eh_0 a}{4}$$

$$\frac{p_0 \pi a^4 e}{4} I\left[\frac{J_3(\sqrt{i\lambda})}{j_1(\sqrt{i\lambda})}\right] = m\Omega^2 y_g (z_g - z_0) - mg y_g$$

$$2\pi p_0 a^2 e^2 \int_0^1 \bar{p}_2\, r\, dr = W \qquad (2.22)$$

From (2.22) we can, for conditions typical of Reiner's experiments, calculate values of x_g and y_g necessary for steady motion as

follows. We assume an h_0 and hence a λ and calculate an e satisfying the last of (2.22), using (2.9) and (2.11) for evaluating $\bar{p}_2$. When e is known, x_g and y_g can be found from the first two of (2.22). For λ small compared with 16, the explicit forms for L, M_x, M_y from (2.14) and (2.19) can be used to simplify calculations. Table below shows the results from such calculations. Here $r_g = \sqrt{x_g^2+y_g^2}$.

Table 2.1

Data: $a = 0.97$ inches

p_0 = atmospheric (15 psi)

$z_g - z_0 = \frac{1}{16}$ inch

Weight of rotor + springload = W = 85 gms.

Speed of rotation = 9000 rpm.

h_0 as measured by Reiner $\simeq$ 6 microns.

Assumed $h_0(\mu)$	λ	e	r_g
12.38	4	0.314	0.025
6.19	16	0.116	0.026
2.47	100	0.075	0.028

It is seen that the value of r_g necessary for steady motion is not critically dependent on h_0 and the center of gravity of the disc should be off axis by about 0.025 inches. Considering Reiner's claim to extreme accuracy in the making of the rotor, an error in rotor centering of this magnitude looks unlikely.

2.2 Analysis of Rotor Stability.

Consider a situation identical with that in Reiner's experiments except for a pivot which keeps the central distance between the two discs constant. Evidently, a steady state with the rotor rotating with its plane parallel to the stator is possible. If such a state is stable and the pivot is removed, the rotor will sink.

But, if the above steady state is unstable, it is possible for another equilibrium state to exist such that the rotor executes oscillations of finite amplitude. Such oscillations produce a lift, which, for an appropriate value of the central distance between the discs, can be equal to the weight of the rotor. Under such conditions, if the pivot is removed, the rotor will not sink.

Thus, instability of the rotor when its center is held at a constant distance from the stator could provide a basis for an investigation of self-excited oscillations. In what follows, we analyze such a possibility.

The pressure p', is governed by the equation (2.1) which on introducing the variables:

$$r = \frac{r'}{a}, \quad t = \Omega t', \quad p = \frac{p'-p_0}{p_0},$$

$$h = \frac{h'}{h_0}, \quad \rho' = \rho_0(1+p), \quad \bar{\theta} = \theta' \tag{2.23}$$

becomes:

$$\frac{\partial}{\partial r}\left(rh^3(1+p)\frac{\partial p}{\partial r}\right)+\frac{\partial}{\partial \bar{\theta}}\left(\frac{1}{r}h^3(1+p)\frac{\partial p}{\partial \theta}\right) = \Lambda r \frac{\partial}{\partial \bar{\theta}}\{(1+p)h\} + 2\Lambda r \frac{\partial}{\partial t}\{(1+p)h\} \tag{2.24}$$

We linearize eqn. (2.24) about the equilibrium solution $p = 0$, $h = 1$ by defining

$$p = \epsilon\, p_1 + O(\epsilon^2)\ , \quad h = 1 + \epsilon\, h_1(r, \bar{\theta}, t) \tag{2.25}$$

where $\epsilon << 1$ and $h_1(r, \bar{\theta}, t)$ is of order unity. We get

$$\frac{\partial}{\partial r}\left(r\, \frac{\partial p_1}{\partial r}\right) + \frac{\partial}{\partial \bar{\theta}} \left(\frac{1}{r}\, \frac{\partial p_1}{\partial \bar{\theta}}\right) = \lambda r\, \frac{\partial p}{\partial \theta} + \lambda r\, \frac{\partial h_1}{\partial \theta} + 2\lambda r\, \frac{\partial h_1}{\partial t} + 2\lambda r\, \frac{\partial p_1}{\partial t} \tag{2.26}$$

Corresponding to the possible oscillations of the rotor in the two degrees of freedom, we choose h_1 to be of the form

$$\epsilon\, h_1 = \alpha(t)\ r\cos\bar{\theta} + \beta(t)\, r \sin\bar{\theta} \tag{2.27}$$

and seek the solution for p_1 in the form

$$\epsilon\, p_1 = F(r,t)\cos\bar{\theta} + G(r,t)\sin\bar{\theta}. \tag{2.28}$$

It is seen that $\frac{h_0 \alpha}{a}$, $\frac{h_0 \beta}{a}$ are the inclinations of the rotor relative to the stator. Using (2.27) and (2.28) in (2.26) we have the equations for F and G as:

$$\frac{\partial}{\partial r}\left(r\, \frac{\partial F}{\partial r}\right) - \frac{F}{r} = \lambda r G + \lambda r^2 \beta(t) + 2\lambda r^2\, \frac{d\alpha}{dt} + 2\lambda r\, \frac{\partial F}{\partial t}$$

$$\frac{\partial}{\partial r}\left(r\, \frac{\partial G}{\partial r}\right) - \frac{G}{r} = -\lambda r F - \lambda r^2 \alpha(t) + 2\lambda r^2\, \frac{d\beta}{dt} + 2\lambda r\, \frac{\partial G}{\partial t} \tag{2.29}$$

Eqns. (2.29) have a particular solution

$$F_p = -\alpha r, \quad G_p = -\beta r \tag{2.30}$$

Writing

$$F = F_p + F_c , \; G = G_p + G_c \tag{2.31}$$

we have equations for F_c, G_c as

$$\frac{\partial}{\partial r}\left(r \frac{\partial F_c}{\partial r}\right) - \frac{F_c}{r} = \lambda r G_c + 2\lambda r \frac{\partial F_c}{\partial t}$$

$$\frac{\partial}{\partial r}\left(r \frac{\partial G_c}{\partial r}\right) - \frac{G_c}{r} = \lambda r F_c + 2\lambda r \frac{\partial G_c}{\partial t} \tag{2.32}$$

The boundary condition corresponding to $p = 0$ at $r = 1$ implies that at $r = 1$,

$$F_c = \alpha(t), \quad G_c = \beta(t) \tag{2.33}$$

For linear stability analysis, we take $\alpha(t)$ and $\beta(t)$ of the form

$$\alpha = R\{\alpha_0 e^{qt}\} , \quad \beta = R\{\beta_0 e^{qt}\} \tag{2.34}$$

where α_0, β_0, q are complex. Corresponding to (2.34) we take F_c, G_c of the form

$$F_c = R\{F_{c0} e^{qt}\} , \; G_c = R\{G_{c_0} e^{qt}\} . \tag{2.35}$$

Equations for F_{c0}, G_{c0}, obtained from (2.32) are

$$\frac{\partial}{\partial r}\left(r\frac{\partial F_{c0}}{\partial r}\right) - \frac{F_{c0}}{r} = \lambda r G_{c0} + 2\lambda\, r q F_{c0}$$

$$\frac{\partial}{\partial r}\left(r\frac{\partial G_{c0}}{\partial r}\right) - \frac{G_{c0}}{r} = \lambda r F_{c0} + 2\lambda r q G_{c0} \tag{2.36}$$

with boundary conditions from (2.33) as:

$$F_{c0}(1) = \alpha_0 \ , \quad G_{c0}(1) = \beta_0 \tag{2.37}$$

It will be seen that (2.36) yields a single Bessel's differential equation for $F_{c0} + iG_{c0}$ whose solution subject to (2.37) is

$$F_{c0} + i G_{c0} = (\alpha_0 + i\beta_0)\ \frac{J_1(\sqrt{i\lambda - 2\lambda q}\ r)}{J_1(\sqrt{i\lambda - 2\lambda q})} \tag{2.38}$$

Similarly from (2.36) we have a Bessels equation for $F_{c0} - iG_{c0}$ whose solution subject to (2.37) is

$$F_{c0} - i G_{c0} = (\alpha_0 - i\beta_0)\ \frac{J_1(\sqrt{-i\lambda - 2\lambda q}\ r)}{J_1(\sqrt{-i\lambda - 2\lambda q})} \tag{2.39}$$

Using (2.38), (2.39), (2.34) and (2.30) in (2.31) we have

$$F = R\left[\left[\tfrac{1}{2}(\alpha_0 + i\beta_0)\left\{-r + \frac{J_1(\sqrt{i\lambda - 2\lambda q}\ r}{J_1(\sqrt{i\lambda - 2\lambda q}}\right\} + (\alpha_0 - i\beta_0)\left\{-r + \frac{J_1(\sqrt{-i\lambda - 2\lambda q}\ r}{J_1(\sqrt{-i\lambda - 2\lambda q})}\right\}\right] e^{qt}\right]$$

$$G = R\left[\left[\frac{1}{2i}(\alpha_0 + i\beta_0)\left\{-r + \frac{J_1(\sqrt{i\lambda - 2\lambda q}\ r)}{J_1(\sqrt{i\lambda - 2\lambda q})}\right\} - \frac{(\alpha_0 - i\beta_0)}{2i}\left\{-r + \frac{J_1(\sqrt{-i\lambda - 2\lambda q}\ r}{J_1(\sqrt{-i\lambda - 2\lambda q})}\right\}\right] e^{qt}\right] \tag{2.40}$$

We now proceed to calculate the moments $M_{x'}$ and $M_{y'}$ on the rotor about the axes ox' and oy'. Since we have neglected fluid inertia, the moments due to stresses in the fluid on the rotor are equal and opposite to those on the stator. It is more convenient to evaluate the moments on the stator because the normal stress in the fluid in contact with the stator is the same as the pressure p. Using this fact, we have,

$$M_{x'} = p_0 a^3 \int_0^{2\pi} \int_0^1 p\, r^2 \sin\bar{\theta}\, dr\, d\bar{\theta} = p_0 \pi a^3 \int_0^1 G(r,t)\, dr \qquad (2.41)$$

Using (2.40) and after some simplification

$$M_{x'} = p_0 \pi a^3 R\left[\left\{\frac{(\alpha_0+i\beta_0)}{8i}\,\frac{J_3(\sqrt{i\lambda-2\lambda q})}{J_1(\sqrt{i\lambda-2\lambda q})} - \frac{(\alpha_0-i\beta_0)}{8i}\,\frac{J_3(\sqrt{-i\lambda-2\lambda p})}{J_1(\sqrt{-i\lambda-2\lambda p})}\right\} e^{qt}\right] \qquad (2.42)$$

and similarly

$$M_{y'} = -p_0 \pi a^3 R\left[\left\{\frac{\alpha_0+i\beta_0}{8}\,\frac{J_3(\sqrt{i\lambda-2\lambda q})}{J_1(\sqrt{i\lambda-2\lambda q})} + \frac{\alpha-i\beta_0}{8}\,\frac{J_3(\sqrt{-i\lambda-2\lambda q})}{J_1(\sqrt{-i\lambda-2\lambda q})}\right\} e^{qt}\right] \qquad (2.43)$$

The equations of motion for the rotor, in a system of coordinates o'x", o'y", o'z" with oz" normal to the plane of the rotor as in Fig. 2 are

$$\begin{aligned} A\,\dot{\omega}_{x''} + C\,\omega_{z''}\,\omega_{y''} &= M_{x''} \\ A\,\dot{\omega}_{y''} - C\,\omega_{z''}\,\omega_{x''} &= M_{y''} \\ C\,\dot{\omega}_{z''} &= M_{z''} \end{aligned} \qquad (2.44)$$

In the above $M_{x''}$, $M_{y''}$, $M_{z''}$ are the moments of external forces about o'x", o'y" and o'z" respectively. C is the polar moment of inertia of the rotor about its axis o'z". A is the moment of inertia of the rotor about a diameter passing through the center of the centering ball in Reiner's experiment. Idealizing the rotor to be a thin disc we have $2A = C = \frac{ma^2}{2}$ where m is the mass of the rotor. $\omega_{x''}$ and $\omega_{y''}$, the angular velocities of the rotor about o'x" and o'y" are related to the inclinations of the rotor, $\frac{\alpha h_0}{a}$ and $\frac{\beta h_0}{a}$, by

$$\omega_{x''} = \frac{\Omega h_0}{a} \frac{d\beta}{dt}, \qquad \omega_{y''} = -\frac{\Omega h_0}{a} \frac{d\alpha}{dt} \tag{2.45}$$

We can rewrite (2.44) in the coordinate system ox', oy', oz'. If we define the torque of external forces about the new axes by $M_{x'}$, $M_{y'}$ and $M_{z'}$, we have the transformation relations, to first order in $\frac{h_0}{a}$

$$M_{z''} = M_{z'} - M_{x'} \frac{\alpha h_0}{a} - M_{y'} \frac{\beta h_0}{a}$$

$$M_{x''} = M_{x'} + M_{z'} \frac{\alpha h_0}{a}$$

$$M_{y''} = M_{y'} + M_{z'} \frac{\beta h_0}{a} \tag{2.46}$$

The angular velocity about oz' can be taken to be a constant equal to Ω. Using this, we have the transformation relations for angular velocities as

$$\omega_{z''} = \Omega - \omega_{x'} \frac{\alpha h_0}{a} - \omega_{y'} \frac{\beta h_0}{a}$$

$$\omega_{x''} = \omega_{x'} + \omega_{z'} \frac{\alpha h_0}{a}$$

$$\omega_{y''} = \omega_{y'} + \omega_{z'} \frac{\beta h_0}{a} \tag{2.47}$$

Using (2.46) and (2.47) in the last of (2.44) we can easily show that $M_{z'}$ is of first order in $\frac{h_0}{a}$. On using this, it follows from (2.46) that, to first order in $\frac{h_0}{a}$, $M_{x''} = M_{x'}$ and $M_{y''} = M_{y'}$. Finally equations (2.44), on retaining only the first order terms in $\frac{h_0}{a}$, become

$$\Omega^2 \frac{m h_0 a}{4} \left\{ \frac{d^2\beta}{dt^2} - 2 \frac{d\alpha}{dt} \right\} = M_{x'}$$

$$\Omega^2 \frac{m h_0 a}{4} \left\{ \frac{d^2\alpha}{dt^2} + 2 \frac{d\beta}{dt} \right\} = M_{y'} \tag{2.48}$$

Using (2.34), (2.42) and (2.43), equations (2.48) can be written as

$$R\left[\frac{ma h_0 \Omega^2}{4} (q^2 \beta_0 - 2q\alpha_0) e^{qt} \right]$$

$$= R\left[p_0 \pi a^3 \left(\frac{\alpha_0 + i\beta_0}{8i} \frac{J_3(\sqrt{i\lambda - 2\lambda q})}{J_1(\sqrt{i\lambda - 2\lambda q})} - \frac{\alpha_0 - i\beta_0}{8i} \frac{J_3(\sqrt{-i\lambda - 2\lambda q})}{J_1(\sqrt{-i\lambda - 2\lambda q})} \right) e^{qt} \right]$$

$$R\left[\frac{ma h_0 \Omega^2}{4} (q^2 \alpha_0 + 2q\beta_0) e^{qt} \right]$$

$$= R\left[p_0 \pi a^3 \left(\frac{\alpha_0 + i\beta_0}{8} \frac{J_3(\sqrt{-i\lambda - 2\lambda q})}{J_1(\sqrt{-i\lambda - 2\lambda q})} + \frac{\alpha_0 - i\beta_0}{8} \frac{J_3(\sqrt{-i\lambda - 2\lambda q})}{J_1(\sqrt{-i\lambda - 2\lambda q})} \right) e^{qt} \right] \tag{2.49}$$

Defining

$$S = \frac{m\Omega^2 h_0}{p_0 \pi a^2} \tag{2.50}$$

and taking the sum and difference of the first and i times the second of equations (2.49), we have

$$(\alpha_0 + i\beta_0)\left[S(q^2 + 2iq) - \frac{J_3(\sqrt{i\lambda - 2\lambda q})}{J_1(\sqrt{i\lambda - 2\lambda q})}\right] = 0$$

$$(\alpha_0 - i\beta_0)\left[S(q^2 + 2iq) - \frac{J_3(\sqrt{-i\lambda - 2\lambda q})}{J_1(\sqrt{-i\lambda - 2\lambda q})}\right] = 0 \tag{2.51}$$

Equations (2.51) are the characteristic equations for the eigenvalues of q and the eigenvectors α_0, β_0. It is seen that two equivalent possibilities exist. They are:

(a) $$\alpha_0 + i\beta_0 = 0 ; \quad S(q^2 + 2iq) = \frac{J_3(\sqrt{-i\lambda - 2\lambda q})}{J_1(\sqrt{-i\lambda - 2\lambda q})}$$

(b) $$\alpha_0 - i\beta_0 = 0 ; \quad S(q^2 - 2iq) = \frac{J_3(\sqrt{i\lambda - 2\lambda q})}{J_1(\sqrt{i\lambda - 2\lambda q})} \tag{2.52}$$

The constant S appearing in the above is in the neighborhood of 0.001 under the conditions of Reiner's experiments. Consequently, we need study equation (2.52) for only small values of S. For the case S = 0, the eigenvalues correspond to $J_3(\sqrt{-i\lambda - 2\lambda q}) = 0$. Since $J_3(z) = 0$ has zeros only on the real axis we see that all the eigenvalues corresponding to $J_3(\sqrt{-i\lambda - 2\lambda q}) = 0$ have negative real parts

and hence represent stable solutions. The eigenvalue corresponding to the root $z = 0$ of $J_3(z) = 0$ is purely imaginary and represents a state of neutral stability.

For small values of S, the eigenvalues of (2.52) are close to those for $S = 0$ and hence represent stable solutions with a possible exception corresponding to the case $z = 0$. We pursue this case further by expanding $J_3(z)$ and $J_1(z)$ in series of z as follows.

$$J_3(z) = \frac{z^3}{48} + O(z^5)$$

$$J_1(z) = \frac{z}{2} + O(z^3) \tag{2.53}$$

Writing

$$q = q_r + i(q_i - \tfrac{1}{2}) \tag{2.54}$$

where q_r, q_i are small compared with unity we find on using the first form in (2.52)

$$q_r = -\frac{9S}{\lambda}; \qquad q_i = \frac{108\,S^2}{\lambda^2} \tag{2.55}$$

The real part of q (i.e. q_r) is negative and implies stability of motion. Consideration of the corresponding eigenfunction shows that the rotor axis approaches the vertical exponentially by spiralling around the vertical axis with an angular velocity nearly equal to half the angular velocity of the rotor.

An interesting possibility is the occurance of instability of the rotor for sufficiently large S. Thus if S is increased from zero we may expect an S, say S_0, at which the equation (2.52) exhibits neutral stability. If this is possible, let the corresponding eigenvalue, which is purely imaginary, be im where m is real. Then (2.52) becomes

$$S_0(-m^2 - 2m) = \frac{J_3(\sqrt{-i\lambda - 2im\lambda})}{J_1(\sqrt{-i\lambda - 2im\lambda})}$$

i.e.

$$-S_0(m^2 + 2m) = \frac{J_3\{i^{\frac{3}{2}}\sqrt{(1+2m)\lambda}\}}{J_1\{i^{\frac{3}{2}}\sqrt{(1+2m)\lambda}\}} \qquad (2.56)$$

The left hand side of (2.56) is real so that for nonzero S_0, we should have a real right hand side. But reference to tables of Bessel's functions for complex argument (McLachlan 1954) shows that the right hand side of (2.56) is never real and we have the surprising result namely that the motion of the rotor is stable for any S.

2.3 Effect of Vibrations.

The rotor in Reiner's apparatus is mounted such that there is no coupling with the drive shaft for rotor motion along the axis or about a diameter. Thus significant vibration cannot be transmitted to it from the drive system. But the drive system can transmit vibrations to the stator through the supporting structure. Such vibrations can arise in the drive system due to several possible reasons.

Dynamic unbalance in the drive train can generate vibrations corresponding to the angular velocities of its members. Since the Reiner's machine has only a pair of shafts running roughly at the same speed, the resulting vibrations correspond roughly to the angular speed of the rotor.

The apparatus employs several ball bearings which can generate vibrations at several frequencies (Moeller 1953). Among the more significant are the ones produced due to a faulty spot on a ball striking the races and the ones due to the balls entering and leaving the loaded zone as the balls roll on. These vibrations have a fundamental frequency typically ten to twenty times the angular speed of the shaft on which the bearings are mounted and are particularly rich in harmonics.

Other possible sources of high frequency vibrations are the angular friction drive which can induce vibrations due to stick-slip phenomenon at the friction surfaces and the electric motor which can induce vibrations of a frequency corresponding to the meshing of its magnetic 'teeth'.

Any such oscillations of the stator induce oscillations of the rotor through the air film. As indicated by the analysis of Saffman and Taylor (1957), the relative motion between the discs can produce a lift on the rotor which may be sufficient to sustain its weight.

To pursue this possibility quantitatively, we consider the idealized problems of a stator of radius a executing simple harmonic oscillations. First we consider stator oscillations normal to itself with an amplitude x_0 at a frequency ω. For studying the motion of the rotor separated from the stator by an air film of mean thickness h_0, it is convenient to define the dimensionless numbers M and N as

$$M = \frac{m\omega^2 h_0}{p_0 \pi a^2} \quad ; \qquad N = \frac{12\mu\omega a^2}{p_0 h_0^2} \tag{2.57}$$

Under conditions corresponding to Reiner's experiments, N is large compared with unity and for this case we can show (Beck et al 1969) that for harmonic oscillations of the rotor, the airfilm behaves like a spring of stiffness $m\omega^2\overline{K}$ in parallel with a dashpot of strength $m\omega\overline{C}$ where

$$\overline{K} = \frac{1}{M}\left[1 - \left(\frac{2}{N}\right)^{\frac{1}{2}}\right]$$

$$\overline{C} = \frac{1}{M}\left(\frac{2}{N}\right)^{\frac{1}{2}} \tag{2.58}$$

Using the above, the relative displacement between the two discs, $y = y_0 \sin(\omega t' + \phi)$, can be related to the displacement of the

stator, $x = x_0 \sin\omega t'$, through the equation of motion for the rotor which can be written in dimensionless form using $\bar{y} = y/x_0$ and $t = \omega t'$ as

$$\frac{d^2\bar{y}}{dt^2} + \bar{C}\,\frac{d\bar{y}}{dt} + \bar{K}\,\bar{y} = -\sin t \qquad (2.59)$$

The behavior of the solution of (2.59) is well known. The amplitude of $\bar{y}$ (i.e. y_0/x_0) tends to 1 as $M \to \infty$ and tends to zero like M as M tends to zero. For M near unity, y_0/x_0 is large.

The value of M in the range of Reiner's experiments, with ω corresponding to the angular speed of rotor is very small ($\simeq 0.001$) and thus $y_0/x_0 << 1$. This implies that vibration of the stator at a frequency equal to the angular speed of the rotor is transmitted to the rotor without loss of amplitude and there is no significant relative motion between them. Further, we can show that the lift on the rotor due to the relative oscillations between the discs is

$$L = \frac{5p_0\pi a^2}{4}\left(\frac{y_0}{h_0}\right)^2\left(1 - \left(\frac{2}{N}\right)^{\frac{1}{2}}\right) \qquad (2.60)$$

For the above case, the lift of the rotor is insignificant for any reasonable x_0/h_0 and cannot possibly resist the weight of the rotor.

For ω corresponding to vibrations induced by imperfections in the bearings, M is comparable to unity and then y_0/x_0 is of order 1. Taking $y_0 = x_0$ and equating the lift of the rotor to its weight, W, we have

$$x_0 = h_0 \left[\frac{4W}{5p_0 \pi a^2} \left(1 - \frac{1}{(2/N)^{\frac{1}{2}}} \right) \right]^{\frac{1}{2}} \tag{2.61}$$

Equation (2.61) estimates an x_0 in the range of 0.5 to 1.0 microns for conditions corresponding to Reiner's experiments.

Next we consider harmonic oscillations of the stator about a diameter. For this case, equation (2.1) can be written as

$$\frac{\partial}{\partial r} \left(rh^3 p \frac{\partial p}{\partial r} \right) + \frac{\partial}{\partial \theta} \left(\frac{ph^3}{r} \frac{\partial p}{\partial \theta} \right) = \lambda \frac{\partial}{\partial \theta} (p r h) + N \frac{\partial}{\partial t} (p r h) \tag{2.62}$$

where

$$p = \frac{p'}{p_0} , \qquad \lambda = \frac{6 \Omega \mu a^2}{p_0 h_0^2} , \qquad N = \frac{12 n \mu a^2}{p_0 h_0^2} \tag{2.63}$$

Here n is the frequency of stator oscillations. The other quantities are defined as in Section 2.1 except that p is the pressure ratio and not the pressure perturbation.

For N very large, the solution of (2.62), valid everywhere except in a small region near the edge r = 1, is obtained by equating the last term of (2.62) to zero as:

$$ph = F(r, \theta) \tag{2.64}$$

If y_0, the maximum amplitude of stator oscillations (at the tip of a diameter), is assumed small compared with h_0, we can take

$$h = 1 + \epsilon r \cos\theta \sin t \tag{2.65}$$

where $\epsilon = y_0/h_0$. Corresponding to (2.64) and (2.65) we take ph, which is symmetric in ϵ, to be

$$ph = 1 + \epsilon^2 f(r, \theta) \tag{2.66}$$

An equation for $f(r, \theta)$ is obtained by taking the time average of equation (2.62) and using (2.65) and (2.66) retaining only terms of order ϵ^2 and smaller. We thus find

$$\frac{\partial^2 f}{\partial r^2} + \frac{1}{r}\frac{\partial f}{\partial r} + \frac{1}{r^2}\frac{\partial^2 f}{\partial \theta^2} = \lambda \frac{\partial f}{\partial \theta} \tag{2.67}$$

The boundary condition at the edge for equations of this type was derived by Pan (1967) by a consideration of the full equations corresponding to (2.62). But we can easily find the correct boundary conditions by a boundary layer type of analysis near the edge which shows that the time average of $p^2 h^3$ is independent of the scaled variable normal to the edge in agreement with Pan (1967). From this we can show that

$$f(1, \theta) = \frac{3}{4}\cos^2\theta = \frac{3}{8} + \frac{3}{8}\cos 2\theta \tag{2.68}$$

Solution of (2.67) with the boundary condition (2.68) is easily seen to be of the form

$$f(r, \theta) = \frac{3}{8} + g(r, \theta) \tag{2.69}$$

where $g(r, \theta)$ is a periodic function of θ. We do not evaluate $g(r, \theta)$

as it does not contribute to the lift of the rotor.

Thus from (2.66), using (2.69), we have

$$ph = 1 + \epsilon^2 \left(\frac{3}{8} + g(r,\theta)\right) \tag{2.70}$$

from which, using (2.65), we have

$$p = 1 - \epsilon\, r\cos\theta \sin t + \frac{3}{8}\epsilon^2 + \epsilon^2 r^2 \cos^2\theta \sin^2 t + \epsilon^2 g(r,\theta)$$

and thus the time average of p is

$$\bar{p} = 1 + \frac{3}{8}\epsilon^2 + \frac{\epsilon^2 r^2}{2}\left(\tfrac{1}{2} + \frac{\cos 2\theta}{2}\right) + \epsilon^2 g(r,\theta) \tag{2.71}$$

The normal force on the rotor, L, is easily obtained to be

$$L = \tfrac{1}{2} p_0 \pi a^2 \left(\frac{y_0}{h_0}\right)^2 \tag{2.72}$$

Based on equation (2.72) and using a reasoning as for axial vibrations we have an estimate for the amplitude of stator vibrations of about 1 micron at the tip of a diameter.

2.4 Discussion.

We considered three possible explanations for Reiner's observations. The first which assumes rotor unbalance was proved to be unreasonable on the basis of Reiner's claim to accuracy in the making of the rotor. The second possibility namely that the rotor was unstable was shown not to exist provided that the disturbances were small. Though this does not rule out self-excited oscillations of finite amplitude, such a possibility looks unlikely. The third which assumes the presence of vibrations does provide a reasonable explanation if we assume that the stator vibrates normal to itself or about a diameter at a sufficiently high frequency with a maximum displacement of about 1 micron. Though the analysis was restricted to sinusoidal oscillations for analytical convenience, it is easy to see that similar results are true for oscillations over a spectrum of frequencies likely to exist in the Reiner's apparatus. Vibrations of the stator about a diameter are particularly likely because the movable part of Reiner's apparatus, which includes the discs and a drive shaft, is supported only at three points with two of them on a horizontal axis. The third support is a worm lacking a gear and is likely to provide freedom of movement due to backlash.

From equation (2.61) we note that for a given amplitude of vibration, the central separation between the discs, h_0, increases with increase in pressure. Also, we may expect increased vibration with increase of rotor speed. This would imply a larger h_0 at higher speeds according to (2.61). Similar conclusions are valid for stator vibrations about a diameter. Reiner's observations are consistent

with the above behavior. Also, there is nothing in Reiner's observations to rule out vibrations of about 1 micron amplitude and the hypothesis of viscoelastic behavior of air looks unreasonable.

REFERENCES - Part I

1. Beck, J. V., Holliday, W. G., and Strodtman, C. L., (1969), Experiment and Analysis of a Flat Disc Squeeze-film Bearing Including Effects of Supported Mass Motion, Journal of Lubrication Technology, Trans. of ASME, Ser. F, Vol. 91, No. 1, pp. 138-148.

2. McLachlan, N. W., (1954), Bessel Functions for Engineers, Oxford University Press.

3. Moeller, K., (1953), Handbook of Noise Control, Ed. Harris, Chapter 24, McGraw-Hill Book Company.

4. Pan, C. H. T., (1967), On Asymtotic Analysis of Gaseous Squeeze-Film Bearings, Journal of Lubrication Technology, Trans. ASME, Ser. F, Vol. 89, No. 3, pp. 245-253.

5. Popper, B., and Reiner, M., (1956), A Centripetal Airpump, British Journal of Applied Physics, 7, p. 452.

6. Reiner, M., (1961), Research on the Cross Stresses in the Flow of Rarified Air, AFOSR 44.

7. Salbu, E. O. J., (1964), Compressible Squeeze Films and Squeeze Bearings, Journal of Basic Engineering, Trans. of ASME, Vol. 86, pp. 355-366.

8. Schlichting, H., (1968), Boundary Layer Theory, 6th Edition, New York: McGraw-Hill.

9. Taylor, G. I., and Saffman, P. G., (1957), Effects of Compressibility at Low Reynolds Number, J. of Aero. Sci., Vol. 28, No. 4, pp. 533-562.

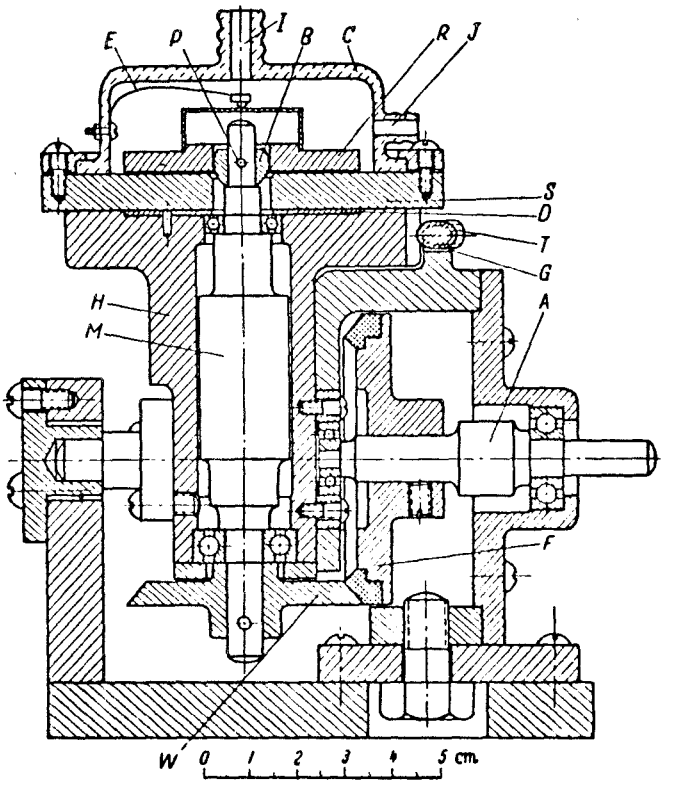

Figure 1
Section of centripetal vacuum pump

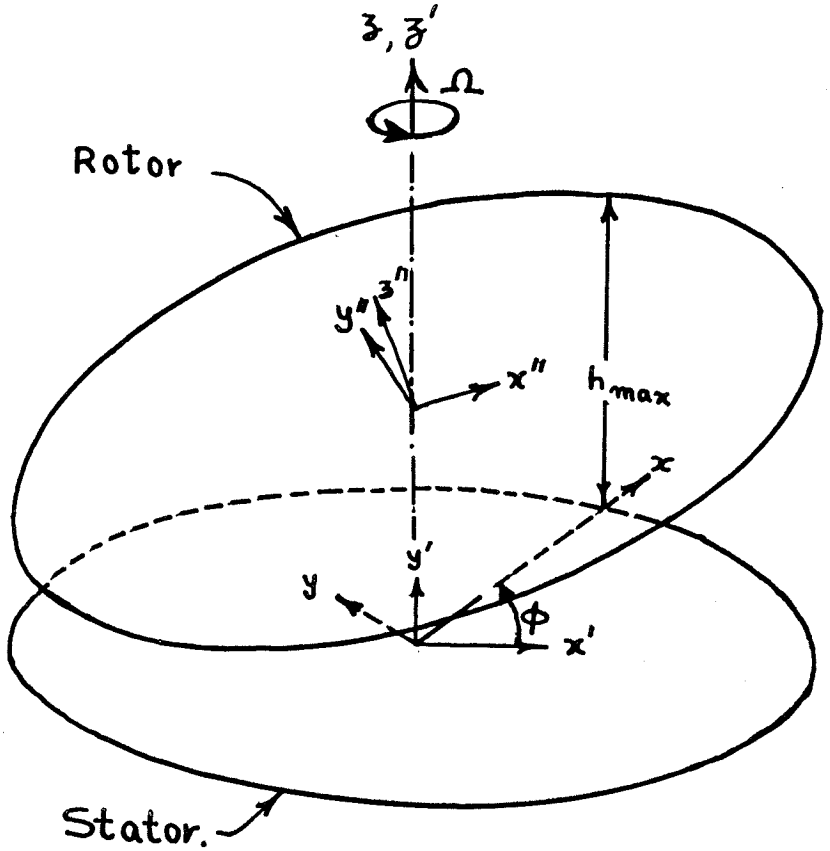

FIG. 2

PART II

A Study of Some Turbulent Flows Using a Model for Inhomogeneous Turbulence

1. The Model

1.1 Introduction.

Turbulent flows are common in nature and include many of practical importance. These flows are highly irregular and complex and it is not practical to analyze these starting from the Navier-Stokes equations. Even the restricted question of predicting only the mean values of the flow quantities is still unanswered.

Any theory of turbulent flow not starting from the Navier-Stokes equations has to make empirical assumptions about the turbulent stresses. Several such theories—among them the mixing length theories of Prandtl and Taylor—have been tried. These simple theories are unsatisfactory in that they involve non-universal constants. For each type of flow, these constants have to be determined from experiments. Thus, these theories can only be considered as a compact means of presenting experimental results. The need for a theory which can be applied to novel situations without the aid of experiments still exists.

Recognizing this need, Prandtl (1945) proposed a one-equation model for turbulence. He assumed that the eddy diffusivity E was proportional to $q\ell$ where q is the amplitude of turbulent fluctuations and ℓ is a length scale characteristic of the mixing due to turbulence. q was determined from an equation roughly corresponding to the turbulent energy equation. The distribution of ℓ was assumed suitably for each type of flow. Spalding (1969) and his co-workers studied some turbulent flows using Prandtl's model. They state that

their applications show the inadequacy of the Prandtl's model.

Harlow and Nakayama (1967) propose a two-equation model roughly similar to the Prandtl's model above with the local length scale ℓ itself being the solution of a second model equation. But they have not applied their model to any real flow situation and the usefulness of their model is still an open question.

Other two equation models include the ones due to Kolmogorov (1942) and Spalding (1969). These models employ two model variables roughly corresponding to the energy density and the vorticity density of the turbulent fluctuations. The eddy diffusivity is taken to be the ratio of energy density to the vorticity density. No application of Kolmogorov's model to any flow is available. The model equations due to Spalding contain a number of free parameters and his applications to some simple flows (i.e. pipe flow, jets) indicate that the free parameters are not universal constants. Thus the usefulness of his model is open to question.

Independently, Saffman (1969) proposed a two-equation model for turbulence. This model describes turbulence in terms of the energy density e and a vorticity density ω and resembles the model due to Kolmogorov. These model equations contain a set of universal constants. It is a remarkable fact that these constants can be determined once and for all from some very general considerations. It is our purpose to see whether these equations provide a satisfactory basis for analyzing turbulent flows. Though it is possible to take into account the effect of compressibility and molecular viscosity by suitable modification of the equations, we confine our attention to turbulent flows of incompressible fluids with zero molecular viscosity.

1.2 The Model Equations.

Turbulence, according to Saffman's model, is characterized by two scalar densities, the 'energy density' e and the 'vorticity density' ω, satisfying non-linear diffusion equations given by:

$$\frac{\partial \omega^2}{\partial t} + u_i \frac{\partial \omega^2}{\partial x_i} = \alpha \omega^2 \left[\left(\frac{\partial u_i}{\partial x_j} \right)^2 \right]^{\frac{1}{2}} - \beta \omega^3 + \frac{\partial}{\partial x_i} \left(\sigma \cdot E \frac{\partial \omega^2}{\partial x_i} \right) \tag{1.1}$$

$$\frac{\partial e}{\partial t} + u_i \frac{\partial e}{\partial x_i} = \alpha^* e \left(2 S_{ij}^2 \right)^{\frac{1}{2}} - e\omega + \frac{\partial}{\partial x_i} \left(\sigma^* E \frac{\partial e}{\partial x_i} \right) \tag{1.2}$$

with

$$S_{ij} = \tfrac{1}{2} \left(\frac{\partial u_i}{\partial x_j} + \frac{\partial u_j}{\partial x_i} \right) \tag{1.3}$$

$$E = e/\omega \tag{1.4}$$

In the above, the u_i are the components of the mean velocity vector. α, α^*, β, σ, σ^* are universal constants.

For the solution of any flow problem, we have, in addition to the model equations above, the equations of conservation of mass and momentum as:

$$\frac{\partial u_i}{\partial x_i} = 0 \tag{1.5}$$

$$\frac{\partial u_i}{\partial t} + u_j \frac{\partial u_i}{\partial x_j} = - \frac{1}{\rho} \frac{\partial p}{\partial x_i} + \frac{\partial}{\partial x_j} (2E S_{ij}) \tag{1.6}$$

It will be observed that the Reynolds stress tensor, $2E\, S_{ij}$,

is described by a scalar eddy diffusivity, E, related to the turbulent densities e and ω by eqn. (2.4). Also, the vorticity equation contains $\left(\partial u_i/\partial x_j\right)^2$ and is thus sensitive to rigid body rotation while the energy equation contains the strain S_{ij} which is not. This is in accordance with the intuitive idea that energy production should not depend on rotation while vorticity should, being related to angular momentum.

The constants α, α^*, β, σ, σ^* are determined once and for all by comparing the solutions obtained by using the model equations with known properties of some simple turbulent flows. From such considerations Saffman found that

$$\alpha^* \simeq 0.3, \quad \sigma = \sigma^* = \tfrac{1}{2}, \quad \frac{5}{3} < \beta < 2, \quad \frac{\alpha^*}{2} < \alpha < \frac{\alpha^*}{\sqrt{2}} \tag{1.7}$$

1.3. Structure of Solutions Near a Solid Wall.

The law of the wall for a turbulent boundary layer states that the mean velocity u depends on the normal distance from a solid wall according to the equation

$$u = \frac{u_*}{k}\left(\log_e \frac{u_* y}{\nu} + B\right) \tag{1.8}$$

u_* is the friction velocity related to wall shear τ_w (i.e $u_*^2 = \tau_w/\rho$). B is a constant which depends on the nature of the wall and is 2.4 for a smooth wall. k is the Karman constant.

A study of the structure of solutions of the model equations (Saffman 1969) shows that near a wall the model equations permit a solution going like:

$$e = \alpha^* u_*^2 + o(1)$$

$$\omega = \frac{\alpha^* u_*}{ky} + o(\frac{1}{y})$$

$$\frac{du}{dy} = \frac{u_*}{ky} + o(\frac{1}{y}) \tag{1.9}$$

where

$$k^2 = \frac{\beta \alpha^* - \alpha}{4\sigma} \tag{1.10}$$

We see that the form of (1.9) agrees with that of (1.8). For the range of parameters given by (1.7), k lies in the range of 0.38 and 0.47. The accepted value of k, 0.41, lies in this range and we consider the model equations satisfactory in this respect. The constant B in (1.7) provides a boundary condition which the solution of model equations has to satisfy at a solid wall.

1.4 The Turbulent-nonturbulent Interface.

The model equations permit a sharp interface between the turbulent and non-turbulent regions. Such interfaces occur in all free turbulent flows. The model equations do not have a length

scale so that the structure of solutions of these equations near the interfaces depend only on local conditions near them. Hence, without loss of generality, we study a plane steady interface at $x = 0$ as in Fig. 1.1(a). The turbulent fluid in the region $x > 0$ entrains the nonturbulent fluid in $x < 0$ at a speed $u(t)$. The fluid velocity parallel to the interface just ahead of it, v_0, may be a constant (as in the case of wakes and jets) or may depend on time corresponding to an interface advancing into an inviscid flow with curvature (e.g. a vortex) or a region of inviscid shear flow. In general the model equations specialized for a plane interface are:

$$\frac{\partial v}{\partial t} + u \frac{\partial v}{\partial x} = \frac{\partial}{\partial x}\left(E \frac{\partial u}{\partial x}\right)$$

$$\frac{\partial e}{\partial t} + u \frac{\partial e}{\partial x} = \alpha^* e \left|\frac{\partial v}{\partial x}\right| - \beta^* e \omega + \frac{\partial}{\partial x}\left(\frac{E}{2} \frac{\partial e}{\partial x}\right)$$

$$\frac{\partial \omega^2}{\partial t} + u \frac{\partial \omega^2}{\partial x} = \alpha \omega^2 \left|\frac{\partial v}{\partial x}\right| - \beta \omega^3 + \frac{\partial}{\partial x}\left(\frac{E}{2} \cdot \frac{\partial \omega^2}{\partial x}\right) \qquad (1.11)$$

We seek a solution of (1.11) for $x > 0$ which has v continuous across the interface at $x = 0$. By trial and error we find that, for small x, the required solution has the form

$$v \sim A_0(t) + A_1(t)\, x \ln x + A_2(t)\, x$$
$$e \sim B_0(t)\, x^2$$
$$\omega \sim \frac{B_0(t)}{u}\, x \qquad (1.12)$$

with

$$A_0(t) = v_0(t), \qquad A_1(t)\, u(t) = \frac{dA_0(t)}{dt} \qquad (1.13)$$

A_2 and B_0 are arbitrary and depend on the still unspecified conditions in the turbulent fluid near the front. These quantities are determined in any specific flow situation by satisfying the appropriate conditions at solid walls or other interfaces bounding the turbulent region.

Typical profiles for v as a function of x for constant t are shown in Fig. 1.1. In general, $\frac{\partial v}{\partial x}$ maintains its sign through the interface and is infinite as we approach the interface from the turbulent side. In the case when v_0 is a constant (as in jets and wakes), $\frac{\partial v}{\partial x}$ is nonsingular. When $\frac{dA_0}{dt} < 0$ corresponding to a diffusing turbulent line vortex, $\frac{\partial v}{\partial x}$ is positive and the tangential velocity near the interface of the expanding vortex is as in Fig. 1.1(b).

The case when u = 0 will not be considered here. Saffman (1969) shows that in this case the interface is noticeably less sharp and for $x > 0$

$$v \sim A_0 + A_1 x^4 \tag{1.14}$$

In Appendix I, we show that the structure of solutions near interfaces obtained above is consistant with the limit of viscous solutions with the viscosity ν tending to zero.

2. Some Applications.

2.1 The Two-dimensional Wake.

We consider a two-dimensional wake with a kinematic momentum defect D. If U is the free stream velocity and u, v are the perturbations, the model equations with boundary layer approximations become

$$\frac{\partial u}{\partial x} + \frac{\partial v}{\partial y} = 0$$

$$U \frac{\partial u}{\partial x} = \frac{\partial}{\partial y}\left(E \frac{\partial u}{\partial y}\right)$$

$$U \frac{\partial e}{\partial x} = \alpha^* e \left| \frac{\partial u}{\partial y} \right| - e\omega + \tfrac{1}{2} \frac{\partial}{\partial y}\left(E \frac{\partial e}{\partial y}\right)$$

$$U \frac{\partial \omega^2}{\partial x} = \alpha \omega^2 \left| \frac{\partial u}{\partial y} \right| - \beta \omega^3 + \tfrac{1}{2} \frac{\partial}{\partial y}\left(E \frac{\partial \omega^2}{\partial y}\right) \qquad (2.1)$$

We seek a similarity solution of this set of equations in the form:

$$\begin{aligned} u &= -D^{\frac{1}{2}} x^{-\frac{1}{2}} F(\eta) \\ e &= D x^{-1} J(\eta) \\ \omega &= U x^{-1} k(\eta) \\ \eta &= U x^{-\frac{1}{2}} D^{-\frac{1}{2}} y \end{aligned} \qquad (2.2)$$

In the similarity variables, equations (2.1) for $\eta < 0$ reduce to

$$\tfrac{1}{2}\left[F(\eta) + \eta F'(\eta)\right] = -\frac{d}{d\eta}\left(\frac{J}{K}\cdot\frac{dF}{d\eta}\right)$$

$$-J - \frac{\eta J'}{2} = \alpha^* JF' - JK + \tfrac{1}{2}\left(\frac{JJ'}{K}\right)'$$

$$-2K^2 - KK'\eta = \alpha K^2 F' - \beta K^3 + (JK')' \qquad (2.3)$$

The first of (2.3) can be integrated once and we can choose the arbitrary constant to satisfy the symmetry condition $F'(0) = 0$ to get

$$\frac{\eta F(\eta)}{2} = -\frac{J}{K} F' \qquad (2.4)$$

We have to solve the last two of (2.3) and (2.4) for the functions F, J, K subject to the symmetry conditions $J'(0) = K'(0) = 0$. Also, we should have a turbulent-nonturbulent interface at $\eta = -\lambda$ where λ is a constant which determines the width of the wake. For convenience in numerical solution we define new variables by the relations

$$\begin{aligned} F(\eta) &= A_0 \overline{F}(\overline{\eta}) \\ J(\eta) &= A_0 \alpha^* \lambda \overline{J}(\overline{\eta}) \\ K(\eta) &= A_0 \alpha^* \lambda^{-1} \overline{K}(\overline{\eta}) \\ \eta &= \lambda \cdot \overline{\eta} \end{aligned} \qquad (2.5)$$

Then (2.4) and the last two of (2.3) become, with $p = A_0 \alpha^*/\lambda$ and $\mu = \alpha/\alpha^*$, A_0 being a constant as yet undetermined,

$$\frac{\overline{\eta}\,\overline{F}}{2} + \frac{\overline{J}\,\overline{F}'}{\overline{K}} = 0$$

$$\overline{J} + \frac{\overline{\eta}\,\overline{J}'}{2} + p\,\overline{J}\,\overline{F}' - p\overline{J}\,\overline{K} + \tfrac{1}{2}\left(\frac{\overline{J}\,\overline{J}'}{\overline{K}}\right)' = 0$$

$$2\overline{K}^2 + \overline{\eta}\,\overline{K}\,\overline{K}' + \mu \cdot p \cdot \overline{K}^2\overline{F}' - \beta p\overline{K}^3 + (\overline{J}\,\overline{K}')' = 0 \qquad (2.6)$$

The structure of solutions of (2.6) near the turbulent-non-turbulent interface at $\overline{\eta} = -1$ is of the type shown in Fig. 1.1(d). We seek series solutions for $\overline{F}$, $\overline{J}$, $\overline{K}$ valid near $\overline{\eta} = -1$ of the form

$$\overline{F} = \xi + A_1\xi^2 + A_2\xi^3 + o(\xi^3)$$

$$\overline{J} = B_0(\xi^2 + B_1\xi^3 + B_2\xi^5) + o(\xi^5)$$

$$\overline{K} = 2B_0(\xi + C_1\xi^2 + C_2\xi^3) + o(\xi^3) \qquad (2.7)$$

where $\xi = \overline{\eta} + 1$. Using the form (2.7) in (2.6) we find that B_0 is arbitrary and the other coefficients are related by the equations:

$$B_1 + A_1 - C_1 + 1 = 0$$

$$B_2 - C_2 + 2A_2 + C_1^2 - B_1C_1 + 2A_1B_1 - 2A_1C_1 + A_1 = 0$$

$$9B_1 - 6C_1 + 4p + 8 = 0$$

$$4B_2 - 2C_2 + 2C_1^2 - 5B_1C_1 + 3B_1^2 + p(2A_1 + B_1 - 2B_0) + \frac{5}{2}B_1 = 0$$

$$6B_1 + 4\mu p + 12 = 0$$

$$2B_2 + 2C_2 + 4B_1C_1 + 2p\mu(A_1 + C_1) - 2\beta B_0 p + 7C_1 - 2C_1^2 = 0 \qquad (2.8)$$

For a B_0 and a p, we can find a unique solution of the set of equations (2.6) exhibiting the structure near $\bar{\eta} = -1$ of the form (2.7). We can choose a B_0 and a p such that the solution so obtained satisfies the symmetry conditions at $\eta = 0$ (i.e. $\bar{J}'(0) = \bar{K}'(0) = 0$). Iterative schemes to obtain such a solution based on Newton's method and the method of steepest descent do not converge and we adopt the following simple but expensive procedure.

We choose a B_0 and a p and integrate the set of equations (2.6) using the Adam-Moulton scheme. We use (2.7) to provide the starting values for the numerical integration, the first point being at -0.95. We record the values of $\bar{J}'(0)$ and $\bar{K}'(0)$ so obtained and repeat the process for several values of B_0 and p. With sufficient data it is possible to plot curves in B_0p plane with $\bar{J}'(0) = 0$ and with $\bar{K}'(0) = 0$. The intersection of these curves provides the desired choice of B_0 and p. The procedure is repeated for various values of α and β as desired. Fig. 2.1 shows one such plot. We observe that the intersection is weak and provides an explanation for the failure of the iterative schemes.

The initial values for numerical integration are obtained from (2.8) and have errors of the order ξ^3. These errors are expected to be less than 1%. The accuracy of numerical integration cannot be easily estimated. Solutions obtained by using the step sizes $\Delta\bar{\eta} = 0.01$ and 0.005 did not show significant differences. The solutions presented are thus believed to be correct to within a few percent at the worst.

The numerical procedure determines $\overline{F}$, $\overline{J}$, $\overline{K}$ which can be related to F, J, K by (2.5). The unknown A_0 in these is determined by the condition of conservation of momentum as below:

$$U \int_{-\lambda}^{\lambda} u \, dy = D$$

$$\text{i.e.} \quad 2A_0 \lambda \int_0^1 \overline{F} \, d\overline{\eta} = 1 \tag{2.9}$$

Also, by definition

$$\frac{A_0 \alpha^*}{\lambda} = p \tag{2.10}$$

From (2.9) and (2.10) we have

$$A_0 = \sqrt{\frac{p}{2\alpha^* \int_0^1 \overline{F} d\overline{\eta}}} \; ; \quad \lambda = \sqrt{\frac{\alpha^*}{2p \int_0^1 \overline{F} \, d\overline{\eta}}} \tag{2.11}$$

Table 2.1

Solution of Model Equations for Wake. $\alpha^* = 0.3$.

β	α	λ	$\lambda_{\frac{1}{2}}$	F(0)	J(0)	K(0)
2.0	0.15	0.71	0.48	1.085	0.442	2.25
1.67	0.21	0.53	0.34	1.53	0.358	2.29
Experiment (Schlichting)			0.354	1.37		

The solution is now complete. Significant results are shown in

Fig. 2.2 and Table 2.1. As the velocity profile obtained from experiments does not have a well-defined edge, it is convenient to compare the estimated growth of the wake with experiments by defining a $\lambda_{\frac{1}{2}}$ related to $y_{\frac{1}{2}}$, the ordinate at any x at which the velocity defect reaches half its value on the axis, as

$$\lambda_{\frac{1}{2}} = U x^{-\frac{1}{2}} D^{-\frac{1}{2}} y_{\frac{1}{2}}$$

It is seen that the wake width is well estimated and the values of the parameters in the permissible zone are best chosen to be $\beta = \frac{5}{3}$ and $\alpha = 0.21$.

2.2 The Two-Dimensional Jet.

For a two-dimensional jet with total (kinematic) momentum flux M, we can seek a similarity solution of the form:

$$\begin{aligned} u &= M^{\frac{1}{2}} x^{-\frac{1}{2}} F'(\eta) \\ v &= M^{\frac{1}{2}} x^{-\frac{1}{2}} (\eta F' - \tfrac{1}{2} F) \\ e &= M x^{-1} J(\eta) \\ \omega &= M^{\frac{1}{2}} x^{-\frac{3}{2}} K(\eta) \\ \eta &= y/x \end{aligned} \qquad (2.12)$$

Here $F(\eta)$ is the stream function. The jet extends from $\eta = -\lambda$ to $\eta = +\lambda$. Using the form (2.12) in the model equations, we have to the boundary layer approximation, for $\eta < 0$,

$$- FF' = \frac{2JF''}{K}$$

$$- JF' - \frac{FJ'}{2} = \alpha^* JF'' - JK + \tfrac{1}{2}(JJ'/K)'$$

$$- 3K^2F' - FKK' = \alpha K^2 F'' - \beta K^3 + (JK')' \qquad (2.13)$$

It is useful to transform variables as below:

$$F(\eta) = A_0 \lambda^{\frac{1}{2}} \bar{F}(\bar{\eta})$$

$$J(\eta) = - \frac{A_0^2 C_1}{2} \alpha \bar{J}(\bar{\eta})$$

$$K(\eta) = A_0 C_1 \lambda^{-\frac{3}{2}} \alpha \bar{K}(\bar{\eta})$$

$$\eta = \lambda(\bar{\eta} - 1) \qquad (2.14)$$

A_0 and C_1 are (negative) constants still underdetermined. In the new variables the equations (2.13) become, with $p = \alpha/\lambda$ and $\Omega = \alpha^*/\alpha$

$$\bar{F}\,\bar{F}' + \frac{2\bar{J}\bar{F}''}{\bar{K}} = 0$$

$$\bar{J}\,\bar{F}' + \frac{\bar{F}\,\bar{J}'}{2} + \tfrac{1}{2}\left(\frac{\bar{J}\,\bar{J}'}{\bar{K}}\right)' + p(\Omega \bar{J}\bar{F}'' - C_1 \bar{J}\,\bar{K}) = 0$$

$$3\bar{K}^2\bar{F}' + \bar{F}\bar{K}\bar{K}' + (\bar{J}\bar{K}')' + p(\bar{K}^2\bar{F}'' - 2C_1\bar{K}^3) = 0 \qquad (2.15)$$

Without loss of generality, solutions of (2.15) near $\bar{\eta} = 0$ can be

taken to be

$$\overline{F} = 1 + A_1\overline{\eta}^2 + A_2\overline{\eta}^3 + o(\eta^3)$$

$$\overline{J} = \overline{\eta}^2 + B_2\overline{\eta}^3 + o(\eta^3)$$

$$\overline{K} = \overline{\eta} + C_2\overline{\eta}^2 + o(\eta^2) \qquad (2.16)$$

On using the form (2.16) in (2.15) we find that A_1 is arbitrary and the rest of the coefficients can be related to A_1, p and C_1. Thus, for every given set of p, A_1 and C_1 we can find a unique solution of (2.15) having a structure near $\eta = 0$ of the form (2.16). We can find a set of values for p, A_1 and C_1 such that the solution so obtained satisfies the symmetry conditions $\overline{J}'(1) = \overline{K}'(1) = 0$ and $F(1) = 0$, the last following from the fact that $v = 0$ at $\overline{\eta} = 1$. We find such a solution by a procedure similar to the one used in the case of the wake. This determines $\overline{F}$, $\overline{J}$, $\overline{K}$. F, J, K can then be found using (2.14). The only unknown in these equations, A_0, is found from the condition of conservation of momentum of the jet:

$$\int_{-\lambda}^{\lambda} u^2\, dy = M$$

$$\text{i.e.} \quad 2A_0^2 \int_0^1 \overline{F}^2\, dy = 1 \qquad \text{or} \qquad A_0 = -\sqrt{\frac{1}{2\int_0^1 \overline{F}^2\, d\overline{\eta}}} \qquad (2.17)$$

We present some results so obtained in Fig. 2.3 and Table 2.2. Data from experiments are presented for comparison. It is

observed that the width of jet is considerably over-estimated by the model equations. The best values for the constants in the model equations are: $\beta = \frac{5}{3}$, and $\alpha = 0.20$.

Table 2.2

Solution of Model Equations for a 2.D Jet. $\alpha^* = 0.3$.

β	α	λ	$\lambda_{\frac{1}{2}}$	F'(0)	J(0)	k(0)
2.0	0.15	0.412	0.214	1.78	0.0278	2.46
2.0	0.20	0.368	0.191	1.89	0.0232	2.78
1.67	0.20	0.29	0.147	2.2	0.0216	4.06
Experiment			0.1	2.68		

2.3 Turbulent Couette Flow.

The flow between two infinite parallel planes at y = -L and y = +L moving parallel to themselves with equal but opposite velocities is of considerable interest because it is possible to solve the model equations analytically. In such a flow, let u_* be the friction velocity at either wall and u(y) be the velocity of the fluid. Then, the model equations reduce to:

$$\frac{e}{\omega}\frac{du}{dy} = u_*^2$$

$$\alpha^* e \frac{du}{dy} - e\omega + \tfrac{1}{2}\frac{d}{dy}\left(\frac{e}{\omega}\cdot\frac{de}{dy}\right) = 0$$

$$\alpha\omega^2\frac{du}{dy} - \beta\omega^3 + \frac{d}{dy}\left(e\frac{d\omega}{dy}\right) = 0 \qquad (2.18)$$

Eliminating $\frac{du}{dy}$ in the second of (2.18) using the first, we have

$$\alpha^* \omega u_*^2 - e\omega + \tfrac{1}{2}\left(\frac{ee'}{\omega}\right)' = 0 \tag{2.19}$$

whose solution satisfying the symmetry condition $de/dy = 0$ at $y = 0$ and the condition at a solid wall $e(L) = \alpha^* u_*^2$ is seen to be

$$e = \alpha^* u_*^2 \tag{2.20}$$

Using (2.20) the last of (2.18) becomes

$$\left(\alpha/\alpha^* - \beta\right)\omega^3 + \alpha^* u_*^2 \frac{d^2\omega}{dy^2} = 0 \tag{2.21}$$

With the notation $\omega(0) = \omega_0$, (2.21), on integration yields

$$\frac{d\omega}{dy} = \sqrt{\frac{\beta - \alpha/\alpha^*}{2\alpha^* u_*^2}} \sqrt{\omega^4 - \omega_0^4} \tag{2.22}$$

Another integration and the use of the boundary condition at the wall $y = L$, which implies $\omega \to \infty$ as $y \to L$

$$\int_{\omega}^{\infty} \frac{d\omega}{\sqrt{\omega^4 - \omega_0^4}} = \frac{\sqrt{\beta - \alpha/\alpha^*}}{\sqrt{2\alpha^* u_*^2}} (L - y) \tag{2.23}$$

ω_0 can be determined easily as $\omega(0) = \omega_0$ which on using (2.23) becomes

$$\int_{\omega_0}^{\infty} \frac{d\omega}{\sqrt{\omega^4 - \omega_0^4}} = L\left(\frac{\beta - \frac{\alpha}{\alpha^*}}{2\alpha^* u_*^2}\right)^{\frac{1}{2}} \tag{2.24}$$

$$\text{i.e.} \qquad \omega_0 = \frac{\int_1^{\infty} \frac{dt}{\sqrt{t^4 - 1}}}{L\left(\frac{\beta - \alpha/\alpha^*}{2\alpha^* u_*^2}\right)^{\frac{1}{2}}} = \frac{1.31}{L\left(\frac{\beta - \alpha/\alpha^*}{2\alpha^* u_*^2}\right)^{\frac{1}{2}}} \qquad (2.25)$$

The integral in the numerator of the above equation is a Jacobian-Elliptic function and its value has been evaluated using tables.

The velocity profile is obtained from (2.18) as follows:

$$\frac{du}{dy} = \frac{\omega}{e} u_*^2 = \frac{\omega}{\alpha^*}$$

Thus

$$u = \int_{\omega_0}^{\omega} \frac{\omega}{\alpha^*} \frac{dy}{d\omega} \, d\omega$$

$$\text{i.e.} \qquad u = \left[\frac{2u_*^2}{\alpha^*(\beta - \frac{\alpha}{\alpha^*})}\right]^{\frac{1}{2}} \int_{\omega_0}^{\omega} \frac{\omega \, d\omega}{\sqrt{\omega^4 - \omega_0^4}} \qquad (2.26)$$

Defining k as in (1.10), we have from (2.26)

$$u = \frac{u_*}{k} \frac{1}{2} \log \left[\left(\frac{\omega}{\omega_0}\right)^2 + \left\{\left(\frac{\omega}{\omega_0}\right)^4 + 1\right\}^{\frac{1}{2}}\right] \qquad (2.27)$$

Equation (2.27) gives u in terms of ω and cannot be presented explicitly in terms of elementary functions of y. However, the behavior of u near the wall y = L can be obtained using asymptotic

expansions valid near the wall. For large ω, (2.27) can be written

$$u = \frac{u_*}{k}\left[\log\sqrt{\frac{\omega}{\omega_0}} - \frac{1}{8(\omega/\omega_0)^2} + \ell n\sqrt{2} + O\left(\frac{1}{(\omega/\omega_0)^4}\right)\right] \tag{2.28}$$

Also using (1.9), for small L - y,

$$\frac{\omega}{\omega_0} = \frac{1}{\omega_0}\,\frac{\alpha^* u_*}{k(L-y)} + o\left(\frac{1}{L-y}\right) \tag{2.29}$$

Equation (2.29) can also be derived directly from (2.23) from which it can be shown that the second term is of order $(L-y)^4$. Use of (2.29) in (2.28) yields

$$u = \frac{u_*}{k}\left[\log\left(\frac{\sqrt{2}}{1.31}\cdot\frac{L}{L-y}\right) + O\left(\frac{L-y}{L}\right)^2\right] \tag{2.30}$$

u_*, the friction velocity at either wall can now be related to the velocity of either wall, U, using the law of the wall which states that near the top wall, assumed smooth,

$$u \sim U - \frac{u_*}{k}\left[\log\frac{u_*(L-y)}{\nu} + 2.4\right] \tag{2.31}$$

From (2.30) and (2.31)

$$U = \frac{u_*}{k}\left[\log\frac{u_* L}{\nu} + \log\frac{\sqrt{2}}{1.31} + 2.4\right] \tag{2.32}$$

Another result of interest is the velocity gradient at y = 0. From (2.18) we have

$$\left.\frac{du}{dy}\right|_0 = \frac{\omega_0}{e} u_*^2 = \frac{1.31\ u_*}{k\ L} \tag{2.33}$$

Robertson (1959) conducted some experiments on the present type of flow using a moving belt apparatus. His results, together with the results of the present analysis are presented in Fig. 2.3.

2.4 Channel flow.

For the flow through a channel with walls at $y = -D$ and $y = +D$, the mean velocity of the fluid $u(y)$ is parallel to the walls and is a function of y alone. Let u_* be the friction velocity at either wall. u_* is related to the pressure gradient along the channel (i.e. $u_* = \left(-\frac{D}{\rho}\frac{dp}{dx}\right)^{\frac{1}{2}}$). The model equations, after some simplification, are, for $y > 0$

$$\frac{e}{\omega}\frac{du}{dy} = -u_*^2\frac{y}{D}$$

$$\tfrac{1}{2}\frac{d}{dy}\left(\frac{e}{\omega}\cdot\frac{de}{dy}\right) = \alpha^* e\left(\frac{du}{dy}\right) + e\omega$$

$$\tfrac{1}{2}\frac{d}{dy}\left(\frac{e}{\omega}\cdot\frac{d\omega^2}{dy}\right) = \alpha\omega^2\left(\frac{du}{dy}\right) + \beta\omega^3 \tag{2.34}$$

By defining

$$y = \bar{y} D$$

$$u = \frac{u_*}{k} \bar{u}$$

$$e = \alpha^* u_*^2 \bar{e}$$

$$\omega = \frac{\alpha^* u_*}{k} \bar{\omega}$$

$$k^2 = \frac{\beta \alpha^* - \alpha}{2} \tag{2.35}$$

the first of the model equations, (2.34), becomes

$$\frac{\bar{e}}{\bar{\omega}} \frac{d\bar{u}}{d\bar{y}} = - \bar{y} \tag{2.36}$$

We can eliminate $\frac{du}{dy}$ from the last two of (2.34) using (2.36). The resulting equations written in terms of the new variables defined in (2.35) are, for $\bar{y} > 0$,

$$\mu \bar{y} \frac{\bar{\omega}^3}{\bar{e}} - \beta \bar{\omega}^3 + \frac{2-\mu}{4} \frac{d}{d\bar{y}} \left(\frac{\bar{e}}{\bar{\omega}} \frac{d\bar{\omega}^2}{d\bar{y}} \right) = 0$$

$$\bar{\omega} \bar{y} - \bar{e} \bar{\omega} + \frac{2-\mu}{4} \frac{d}{dy} \left(\frac{\bar{e}}{\bar{\omega}} \frac{d\bar{e}}{d\bar{y}} \right) = 0 \tag{2.37}$$

where $\mu = \alpha/\alpha^*$. The equations (2.36), (2.37) together with the symmetry conditions $\bar{e}'(0) = \bar{\omega}'(0) = 0$ and the wall conditions at $\bar{y} = 1$ determine a complete solution.

One way of obtaining such a solution is to start a series solution from the wall and continue it towards the center $\bar{y} = 0$ using a numerical method. As an illustration, we consider a specific case when $\mu = 0.5$ and $\beta = 2$. Defining $\xi = 1-\bar{y}$, we find that (2.37) permit a series solution near $\bar{y}=1$ of the form:

$$\bar{e} = 1 + A_1\xi + A_2\xi^{\sqrt{8/3}} + A_3\xi^2 + A_4\xi^{1+\sqrt{8/3}} + A_5\xi^3 + A_6\xi^{2\sqrt{8/3}} + A_7\xi^{2+\sqrt{8/3}} + A_8\xi^4 \ln\xi + A_9\xi^4 + \cdots$$

$$\bar{\omega} = \frac{1}{\xi}\Big(1 + B_1\xi + B_2\xi^{\sqrt{8/3}} + B_3\xi^2 + B_4\xi^{4\sqrt{8/3}} + B_5\xi^3 + B_6\xi^{2\sqrt{8/3}} + B_7\xi^{2+\sqrt{8/3}} + B_8\xi^4 \ln\xi + B_9\xi^4 + \cdots\Big) \qquad (2.38)$$

We find that A_2 and B_9 are arbitrary and all other coefficients can be determined in terms of these. In principle one can determine the constants A_2 and B_9 by extending the series solution by a numerical method and applying the two symmetry conditions $\bar{e}' = \bar{\omega}' = 0$ at $\xi = 1$. For sufficient accuracy we have to keep terms in the series up to at least one power higher than the term where the second arbitrary constant occurs. This means that we have to keep at least fifteen terms in each series. After considerable effort this approach is given up because the chances of algebraic error are extremely large and it has not been possible to obtain the required solution. It may be remarked here that the index of the first fractional power in the above series depends on μ and is $\sqrt{4/2-\mu}$.

An alternative is to shoot from the center towards the wall $\bar{y} = 1$.

Following this approach we consider series solutions of (2.37) near $\bar{y} = 0$ of the form:

$$\bar{e} = C_0\left(1 + C_1\bar{y}^2 + C_2\bar{y}^4 + \cdots\right)$$

$$\bar{\omega} = D_0\left(1 + D_1\bar{y}^2 + D_2\bar{y}^4 + \cdots\right) \qquad (2.39)$$

On using (2.39) in (2.37) we find that C_0, D_0 are arbitrary and other constants are related to them. We can integrate equations (2.37) using (2.39) to provide the initial values. For arbitrary values of C_0 and D_0, the solutions of (2.37) are divergent. At some $\bar{y}$, $\bar{\omega}$ tends to $+\infty$ while $\bar{e}$ tends to + or - ∞ at the same point. By trial and error we can find a close pair of values for C_0 and D_0 such that the solutions so obtained are such that $\bar{\omega} \to +\infty$ as $\bar{y} \to 1$ and $\bar{e} \to +\infty$ for the first pair of values and $-\infty$ for the second pair as $\bar{y} \to 1$. When the pair of values for C_0 and D_0 are sufficiently close we have a good approximation to the required solution of (2.37) away from $\bar{y} = 1$. Though the procedure discussed earlier is potentially more accurate than the one considered here, the present procedure has the great virtue of being practical. This procedure was applied to the Couette flow of the previous section for which the analytical solution is known and satisfactory accuracy was obtained thus establishing the feasibility of this scheme.

Once $\bar{e}$, $\bar{\omega}$ are determined, we can find $\bar{u}$ by integrating (2.36) as below.

$$\bar{u}(\bar{y}) = \bar{U} - \int_0^{\bar{y}} \frac{\bar{\omega}\,\bar{y}}{\bar{e}}\, d\bar{y} \qquad (2.40)$$

$\overline{U} = \overline{u}(0)$ is the dimensionless form of the velocity at the center of the channel U, to be determined such that $\overline{u}$ satisfies the law of the wall at $\overline{y} = 1$ which is, with $\xi = 1-\overline{y}$,

$$\overline{u}(\xi) = \log \xi + 2.4 + \log \frac{u_* D}{\nu} \tag{2.41}$$

It is not convenient to determine $\overline{U}$ by directly comparing (2.40) and (2.41). We proceed by considering the integral I below. As $\frac{d\overline{u}}{d\xi}$ is no more singular than $\frac{1}{\xi}$, the integral exists as $\epsilon \to 0$.

$$\begin{aligned} I &= \int_\epsilon^1 \frac{d}{d\xi}\left(\xi \frac{d\overline{u}}{d\xi}\right) \log \xi \, d\xi \\ &= \log \xi \; \xi \frac{d\overline{u}}{d\xi} \Big|_\epsilon^1 - \int_\epsilon^1 \frac{d\overline{u}}{d\xi} \, d\xi \\ &= -\log \epsilon \left(\xi \frac{d\overline{u}}{d\xi}\right)_\epsilon - \overline{U} + \overline{u}(\epsilon) \end{aligned}$$

$\overline{u}(\epsilon)$ is eliminated using the law of the wall (2.41) to get

$$I = -\log \epsilon \left(\xi \frac{d\overline{u}}{d\xi}\right)_\epsilon - \overline{U} + \log \epsilon + 2.4 + \log \frac{u_* D}{\nu} \tag{2.42}$$

Comparing terms of equal orders in ϵ in (2.42), I being of order 1, we have

$$\overline{U} = 2.4 + \log \frac{u_* D}{\nu} - I$$

and

$$\left(\xi \frac{du}{d\xi}\right)_0 = 1. \tag{2.43}$$

The second of (2.43) is already satisfied by the solution as can be easily verified from (2.36) using (2.38). The first of (2.43) is the required relation between $\overline{U}$ and u_*. The integral I is evaluated as below

$$I = \int_0^1 \frac{d}{d\xi}\left(\xi \frac{\overline{\omega}}{e}(1-\xi)\right) \log \xi \, d\xi$$

$$= \int_0^{0.1} \frac{d}{d\xi}\left(\xi \frac{\overline{\omega}}{e}(1-\xi)\right) \log \xi \, d\xi + \int_{0.1}^1 \frac{d}{d\xi}\left(\xi \frac{\overline{\omega}}{e}(1-\xi)\right) \log \xi \, d\xi$$

We evaluate the first part of the integral using only the first two terms of the series (2.38) and the second part using the numerical solution already described. We find that $I \simeq 0.2$. Thus, the first of (2.43) written in original variables becomes

$$U = \frac{u_*}{k} \left(\log \frac{u_* D}{\nu} + 2.20\right)$$

This should be compared with experimental observations (Hinze 1961) which give

$$U = \frac{u_*}{k} \left(\log \frac{u_* D}{\nu} + 2.4 + C\right)$$

where C is a positive constant whose magnitude is somewhat uncertain. C lies in the range 0 to 1 with a probable value of around 0.25. The analysis implies a C equal to -0.2. The disagreement between analysis and experiment is quantitatively small and we do not consider it to be very significant.

2.5 Discussion.

In the previous sections we considered some simple flows involving either solid walls or free boundaries. In all cases the broad features of the flows are well represented by the model equations. Quantitative agreement with experimental results is fair.

In the case of free turbulent flows, the model equations were solved assuming the turbulent-nonturbulent interfaces, which are always sharp, to be steady. Experiments indicate that the interfaces are sharp but unsteady on a time scale large compared with that of the turbulent fluctuations. When velocities averaged over a long period of time are considered, the unsteadiness is lost and we obtain a smooth transition from the turbulent to the nonturbulent regions. Thus, when the velocity profiles derived from the model equations with the assumption of steady interfaces are compared with the long time mean velocity profiles obtained from experiments, we find poor agreement near the free edges as in Fig. 2.2.

If the model equations are to describe the unsteady nature of the observed flows, two possibilities exist.

(1) The model equations permit unsteady interfaces in the problems considered. This would imply instability of the steady solutions of the previous sections.

(2) The model equations, as presented, are inadequate so that they need modifications to describe the unsteadiness of the flows considered.

At present it is not obvious which of these possibilities is the right one. An analysis of stability of the steady flows obtained

in Sections 2.1 and 2.2 is of interest in this connection. It is interesting to note that if the steady wake of section 2.1 is assumed to oscillate with the point of velocity maximum distributed uniformly in $-0.8 \leq \eta/\eta_{\frac{1}{2}} \leq 0.8$, the mean velocity profile so obtained fits the experimental results much better as in Fig. 2.2. Also, we can estimate the distribution of intermittency based on the above assumption. For convenience in comparison with experiments, we define the edge of the wake as the point at which the velocity defect falls to 0.5% of its value on the axis. We immediately see that the oscillations assumed above lead to a distribution of the intermittancy factor of unity from the axis to a point 0.4 of the distance to the edge. Beyond this point, the intermittency factor falls linearly to zero at the edge. A good approximation to the measured distribution of the intermittency factor (Townsend 1956) is found to be unity up to a point 0.4 of the distance to the edge. Beyond this point, the intermittency factor falls roughly linearly to zero at a point slightly beyond the defined edge.

A similar oscillation of the jet of Section 2.2 with amplitude $0.6\ \eta/\eta_{\frac{1}{2}}$ leads to good agreement of the mean velocity profile with experiments as in Fig. 2.3. The intermittency factor based on these oscillations is unity up to 0.52 of the way to the edge and falls off linearly to zero beyond. A good approximation to the distribution of the intermittency factor obtained from experiment (Bradbury 1965) is unity up to 0.55 of the distance from the axis to the edge and falls roughly linearly to zero slightly beyond the defined edge.

The above agreement is sufficiently good to suggest instability of the steady solutions of Sections 2.1 and 2.2 to be more likely than

the inadequacy of the model equations.

3. The Turbulent Trailing Vortex.

3.1 Introduction.

The flow some distance downstream of an aircraft wing consists of two nearly axi-symmetric contrarotating vortices and a wake extending across the span. The trailing vortices are invariably turbulent and persist for a long distance downstream of the wing. It is useful to know the flow field due to these so that their effect on other aircraft that might accidentally penetrate them can be assessed.

In the zone of interest, it is observed that the diameter of each vortex is small compared with the distance between them. Thus it is possible to study each vortex in isolation. Dimensional reasoning indicates that a similarity type of solution is possible for each vortex. Such a solution can be written in the form

$$\frac{\Gamma}{\Gamma_0} = f(\eta; \frac{\Gamma_0}{\nu}) \tag{3.1}$$

where

$$\eta = \frac{r}{\sqrt{\Gamma_0 Z/U}} \tag{3.2}$$

In the above, Γ is the circulation of the vortex at a radial distance r. Γ_0, the circulation as $r \to \infty$, is independent of the axial distance, Z, measured from a virtual origin close to the position of the wing. U is the free stream velocity. Γ_0/ν is a Reynolds number and is in the range of 10^6 to 10^7 for typical aircraft. Incidentally, $\frac{Z}{U}$ represents

a time. Denoting it by t, we note that the equations (3.1) and (3.2) also represent the form of solution for the growth of a line vortex in time.

Lamb (1932) solved the problem of diffusion of a laminar line vortex and his solution in the present notation is

$$\frac{\Gamma}{\Gamma_0} = 1 - \exp\left[\frac{-\eta^2}{4\left(\frac{\nu}{\Gamma_0}\right)}\right] \tag{3.3}$$

This solution shows a region of rigid body rotation close to the center $\eta = 0$ where the tangential velocity, u, increases linearly with radius. With further increase in η, u reaches a maximum and then decreases to zero as $\frac{1}{\eta}$ as $\eta \to \infty$. If we define a 'core circulation' Γ_1 and a 'core radius' r_1 as the circulation and the radius where the tangential velocity is the maximum, we have, from (3.3), $\Gamma_1/\Gamma_0 = 0.716$.

Turbulent trailing vortices have been studied experimentally. Full scale experiments to estimate the maximum velocity in the trailing vortex of a large airplane were conducted by Rose and Dee (1965). A small airplane equipped with an incidence meter (i.e. a pivoted vane) was flown through the eye of the vortex (made visible by the use of smoke) shed from a large airplane. Estimates of the maximum velocity in the vortex at various distances along the axis were made using the incidence data from the small airplane. It was found that the maximum velocity fell like $1/\sqrt{Z}$ in agreement with equation (3.1). Further, the maximum velocity was found to be correctly estimated by equation (3.3) if ν in it was replaced by an

eddy viscosity ν_t such that $\nu_t/\nu \simeq 2000$. McCormick et al (1968) studied the flow in a vortex shed from a small airplane by using an instrument labeled the vortimeter. The vortimeter, consisting of a vertical array of horizontal cylinders mounted on strain-gauge flexures, was mounted at a suitable height above the ground. By flying the airplane to one side and suitably above the instrument, it was possible to arrange the vortex to sweep across the instrument, this being aided visually by a tuft grid mounted suitably close by. From the strain gauge data it was possible to estimate the velocity and hence circulation distribution in the vortex at various distances from the airplane. These estimates agree with the similarity form (3.1) with Γ_0 roughly 45% of the maximum circulation on the wing of the airplane calculated on the basis of its speed and weight. This indicates that in the process of roll up of the nearly plane vortex sheet behind the wing into the trailing vortices farther away, only about 45% of the total circulation is concentrated into the vortices, the rest being diffused into the wake.

Following Squire (1954), McCormick et al compared their estimates of the circulation distribution with a solution obtained by replacing ν in Lamb's solution by an eddy viscosity ν_t as:

$$\frac{\Gamma}{\Gamma_0} = 1 - \exp\left(\frac{-\eta^2}{4a}\right) \tag{3.4}$$

where $a = \nu_t/\Gamma_0$ is some function of Reynolds number $\frac{\Gamma_0}{\nu}$. Equation (3.4) implies a $\frac{\Gamma_1}{\Gamma_0} = 0.716$ while the estimate from the experiments is 0.365 indicating poor agreement between the two circulation profiles.

Dosanjh et al (1962) conducted some experiments on turbulent trailing vortices in a wind tunnel. A wing of rectangular plan form was mounted normal to a side wall of a wind tunnel. Measurements of flow inclination were made in the trailing vortex using a five hole flow direction probe. From the flow direction and total pressure data, the axial and tangential velocity distributions were calculated. The circulation distribution so obtained agreed with the form (3.1). Further, the circulation of the vortex, Γ_0, was found to be about 58% of the value at the root of the wing producing the vortex. This is not too far from the flight test data of McCormick.

Results from other similar experiments (see Table 3.1) also indicate agreement with the form (3.1). The growth rate of the vortices as indicated by a ν_t/Γ_0 obtained by equating the estimated maximum velocity in the experiments with that given by equation (3.4) is shown in Table 3.1. It is seen that there is reasonable consistancy among the results of various experiments. As Γ_0/ν increases, ν_t/Γ_0 steadily decreases and we expect its value to reach a limit independent of Γ_0/ν for a sufficiently large value of the same. Rose and Dee obtained the ν_t/Γ_0 in the table by assuming that the maximum circulation at the wing was equal to the circulation of the vortex. In the light of experimental results already quoted we recalculate its value assuming that the circulation of the vortex is one half that at the wing and find $\nu_t/\Gamma_0 = 1.4 \times 10^{-4}$. This reduces some of the disagreement with McCormick's data shown in the table. The considerable disagreement which still persists between these sets of flight data is still unexplained. It is to be noted that though the

value of ν_t is based on the profile given by equation (3.4) which does not fit the profiles from experiments, this ν_t still indicates a measure of vortex growth and is a valid basis for comparing the results from various experiments.

Table 3.1

Experimenter	$\frac{\Gamma_0}{\nu}$	$a = \frac{\nu_t}{\Gamma_0}$	$\frac{\Gamma_1}{\Gamma_0}$
*Rose and Dee	$\sim 10^7$	2×10^{-4}	–
*Rose and Dee (corrected)	$\sim 10^7$	1.4×10^{-4}	–
†Dosanjh, Gesparek and Eskinazi	2×10^3	5×10^{-3}	0.6
†Newman	2×10^4	2×10^{-3}	0.5
†Templin	5×10^4	1.4×10^{-3}	–
†Maybey	5×10^4	1.5×10^{-3}	–
*McCormick, Tangler and Sherrieb	$\sim 10^6$	0.6×10^{-4}	0.37

* Flight results. † Wind tunnel data.

Hoffman and Joubert (1962) present an analysis of the turbulent line vortex. They derive a universal law for the distribution of circulation valid in some region including the center near which circulation increases as the square of the radius and corresponds to rigid body rotation. In some region away from the center the universal distribution gives a logarithmic variation as

$$\frac{\Gamma}{\Gamma_1} = \frac{1}{H} \log_{10}\left(\frac{r}{r_1}\right) + 1 \qquad (3.5)$$

Γ_1, r_1 are the core circulation and core radius respectively. $\frac{1}{H}$ is a constant which they find by comparison with their own experiments to be 2.14 . We note that $\frac{1}{H}$ should be $\log_e 10 (= 2.303)$ for equation (3.5) to satisfy the definition of r_1 (i.e. tangential velocity should be a maximum at radius r_1).

Hoffman and Joubert obtain (3.5) by two methods. The first involves the following assumptions.

(1) Turbulent shear stress can be estimated by a mixing length hypothesis. If small lumps of fluid are assumed to be transported over a small radial mixing length maintaining their angular momentum, it is easily shown that the shear stress $\tau \propto \frac{1}{r} \frac{\partial (vr)}{\partial r}$.

(2) In the region of interest the inertia terms in the tangential momentum equation can be neglected so that shear moment transmitted $(\propto \tau r^2)$ is a constant.

The first assumption describes some free turbulent flows well and may do so in the present case. The second is exact at the point where tangential velocity is a maximum and is likely to be reasonable in some neighborhood of this point.

The second way of deriving (3.5) in effect assumes that the flow inside the core follows a universal form independent of the conditions farther out so that $\frac{\Gamma}{\Gamma_1}$ is a unique function of $\frac{r}{r_1}$. Further, it is claimed that $\frac{d\Gamma}{dr}$ should be independent of r_1 which immediately leads to the form (3.5). The explanations provided by Hoffman and Joubert to justify this claim are very unconvincing.

Comparison of results from experiments already described with equation (3.5) shows good agreement throughout the vortex

though there seems to be some disagreement near the outer edge of the vortex. A typical comparison is shown in Fig. 3.1. However, Fig. 3.1 also shows that equation (3.4) corresponding to constant eddy viscosity also satisfies (3.5) throughout the core (i.e. $r < r_1$) and some distance beyond. Thus good agreement between the form (3.5) and experiments does not necessarily imply the correctness of the hypotheses of Hoffman and Joubert. As the agreement is good, we accept equation (3.5) as an empirical result valid throughout the vortex with the exclusion of small regions near the center and outer edge. We can write (3.5) in the form:

$$\frac{\Gamma}{\Gamma_0} = \frac{\Gamma_1}{\Gamma_0} \frac{1}{H}\left(\log_{10} \frac{r}{r_1} + 1\right) \tag{3.6}$$

which indicates that the slope of circulation profile plotted as a function of $\log r$ depends linearly on Γ_1/Γ_0. As already noted, Γ_1/Γ_0 is considerably different for laminar and turbulent vortices and hence their profiles disagree in this plot.

Another aspect of vortex flow is the variation of a with Reynolds number Γ_0/ν. Owen (1964) presents an analysis using an integral method to explain the observed variation of a with Γ_0/ν. But his analysis has a significant algebraic mistake and his conclusions are invalid. We do not study this problem here.

An interesting secondary effect of the trailing vortex flow is the generation of an axial pressure gradient. Low pressure is produced near the axis of the vortex due to centrifugal acceleration of fluid in it. As the tangential velocity in the vortex decays with axial

distance, suction near the axis of the vortex is reduced and thus we have a positive axial pressure gradient in the core of the vortex. This pressure gradient induces an axial velocity defect very much resembling an ordinary wake. Batchelor (1964) studied the development of axial velocity defect in a laminar trailing vortex assuming that the perturbation of axial velocity is small compared with the free stream velocity. This assumption is satisfied in the later stages of vortex growth. In the early stages of growth, the axial velocity defect is not small compared with free stream velocity and may significantly affect the development of the vortex itself.

In what follows we treat the problem of flow in a fully turbulent trailing vortex on the basis of the model equations to see whether they predict the growth of the trailing vortex satisfactorily. We also consider the details of axial flow using linearization of the axial momentum equation.

3.2 Analysis Based on Model Equations.

For the flow in a turbulent axisymmetric trailing vortex, let r, z, ϕ be the radial, axial and tangential coordinates. Let the corresponding velocities be u_r, u_z and u_ϕ. Let U be the free stream velocity and p the pressure at any point. The model equations under the boundary layer approximation ($\partial/\partial r >> \partial/\partial z$) with the additional assumption of small axial velocity defect ($|u_z - U| << U$) become:

$$\frac{u_\phi^2}{r} = \frac{1}{\rho}\frac{\partial p}{\partial r}$$

$$U\frac{\partial u_z}{\partial z} = -\frac{1}{\rho}\frac{\partial p}{\partial z} + \frac{1}{r}\frac{\partial}{\partial r}\left(\frac{e}{\omega} r \frac{\partial u_z}{\partial r}\right)$$

$$U\frac{\partial u_\phi}{\partial z} = \frac{1}{r^2}\frac{\partial}{\partial r}\left(\frac{e}{\omega} r^3 \frac{\partial}{\partial r}\left(\frac{u_\phi}{r}\right)\right)$$

$$U\frac{\partial \omega^2}{\partial z} = \alpha\omega^2\left|\frac{\partial u_\phi}{\partial r}\right| - \beta\omega^3 + \frac{1}{r}\frac{\partial}{\partial r}\left(\frac{r}{2}\frac{e}{\omega}\frac{\partial \omega^2}{\partial r}\right)$$

$$U\frac{\partial e}{\partial z} = \alpha^* e r\left|\frac{\partial}{\partial r}\left(\frac{u_\phi}{r}\right)\right| - e\omega + \frac{1}{r}\frac{\partial}{\partial r}\left(\frac{r}{2}\frac{e}{\omega}\frac{\partial e}{\partial r}\right) \qquad (3.7)$$

We note that the last three of (3.7) determine u_ϕ, e and ω while the first two determine p and u_z when u_ϕ, e and ω are known. This uncoupling of tangential velocity is due to the assumption of small axial velocity defect and is valid for sufficiently large z.

Equations (3.7) permit a similarity solution for u_ϕ, e and ω of the form

$$u_\phi = \sqrt{\frac{\Gamma_0 U}{z}}\, F(\eta)$$

$$e = \frac{\Gamma_0 U}{z}\, J(\eta)$$

$$\omega = \frac{U}{z}\, K(\eta) \qquad (3.8)$$

with

$$\eta = r\sqrt{U}\,/\sqrt{\Gamma_0 z} \qquad (3.9)$$

Γ_0 is the circulation of the vortex outside the turbulent region which extends from $\eta=0$, the center of the vortex, to $\eta=\lambda$, the turbulent-nonturbulent interface. In the similarity variables equations (3.7) yield

$$\frac{1}{\eta^2}\frac{d}{d\eta}\left\{\frac{\eta J}{K}(\eta F'-F)\right\} + \tfrac{1}{2}(F+\eta F') = 0$$

$$\frac{1}{\eta}\frac{d}{d\eta}(\eta JK') + \alpha K^2|F'| - \beta K^3 + 2K^2 + KK'\eta = 0$$

$$\frac{1}{\eta}\frac{d}{d\eta}\left(\frac{\eta JJ'}{2K}\right) + \alpha^*\eta J\left|\frac{d}{d\eta}\left(\frac{F}{\eta}\right)\right| - JK + J + \frac{J'\eta}{2} = 0 \qquad (3.9)$$

We seek the solution of this set of equations which is non-singular as $\eta \to 0$ and has a sharp interface at some λ. It is convenient to define new variables and parameters as below:

$$F = A_0\bar{F}(\bar{\eta})$$

$$J = A_0\alpha^*\lambda\bar{J}(\bar{\eta})$$

$$K = A_0\alpha^*\lambda^{-1}\bar{K}(\bar{\eta})$$

$$\eta = \lambda\bar{\eta}$$

$$q = \alpha^* A_0\lambda^{-1}$$

$$\mu = \alpha/\alpha^* \qquad (3.10)$$

A_0 is a constant still undetermined. In the new variables (3.9) become:

$$\frac{1}{\bar{\eta}^2}\frac{d}{d\bar{\eta}}\left\{\frac{\bar{\eta}\bar{J}}{\bar{K}}(\bar{\eta}\bar{F}-\bar{F})\right\} + \tfrac{1}{2}\left\{\bar{F} + \bar{\eta}\bar{F}'\right\} = 0$$

$$\frac{1}{\bar{\eta}^2}\frac{d}{d\bar{\eta}}(\bar{\eta}\bar{J}\bar{K}') + q\left\{\mu\bar{K}^2|\bar{F}'| - \beta\bar{K}^3\right\} + 2\bar{K}^2 + \bar{K}\bar{K}'\bar{\eta} = 0$$

$$\frac{1}{\bar{\eta}}\frac{d}{d\bar{\eta}}\left(\frac{\bar{\eta}\bar{J}\bar{J}'}{2\bar{K}}\right) + q\left\{\bar{\eta}\bar{J}\left|\frac{d}{d\bar{\eta}}\left(\frac{\bar{F}}{\bar{\eta}}\right)\right| - \bar{J}\bar{K}\right\} + \bar{J} + \frac{\bar{J}'\bar{\eta}}{2} = 0 \qquad (3.11)$$

Near $\bar{\eta} = 1$, the interface, equations (3.11) have the structure, with $\xi = 1-\bar{\eta}$, as below.

$$\bar{F} \sim 1 + A_1\xi\ln\xi + A_2\xi + A_3\xi^2\ln\xi + A_4\xi^2$$

$$\bar{J} \sim B_0(\xi^2 + B_1\xi^3\ln\xi + B_2\xi^3)$$

$$\bar{K} \sim 2B_0(\xi + C_1\xi^2\ln\xi + C_2\xi^2) \qquad (3.12)$$

Use of (3.12) in (3.11) leads to recurrence relations among the various coefficients. We find that A_2 and B_0 are arbitrary and given these all the others can be calculated. Thus for any given set of A_2, B_0 and q, a unique solution of (3.11) can be found by numerical integration of (3.11) using (3.12) to provide the initial values at some $\bar{\eta}$ near unity. Such a solution is, in general, singular as $\bar{\eta} \to 0$. The solution we are after, which is nonsingular at $\bar{\eta} = 0$, also satisfies symmetry conditions $\bar{F}(0) = \bar{J}'(0) = \bar{K}'(0) = 0$. To get the required solution we choose, by trial and error, a set of values for A_2, B_0 and q such that the symmetry conditions are satisfied to a reasonable degree of accuracy.

Execution of the above scheme determines $\overline{F}$, $\overline{J}$ and $\overline{K}$. F, J and K can then be found using (3.10). The only unknown in these, A_0, is found by equating the circulation at $\eta = \lambda$ to Γ_0 as below:

Circulation at any radius r is

$$\Gamma = 2\pi u_\phi r = 2\pi \Gamma_0 \bar{F} \eta$$

$$= 2\pi \Gamma_0 A_0 \lambda \overline{F}\, \overline{\eta} \qquad (3.13)$$

Thus $\Gamma = \Gamma_0$ at $\overline{\eta} = 1$ implies

$$2\pi A_0 \lambda = 1 \qquad (3.14)$$

Also, by definition,

$$q = \alpha^* A_0 / \lambda \qquad (3.15)$$

From (3.14) and (3.15) we have

$$A_0 = \sqrt{\frac{q}{2\pi \alpha^*}} \; ; \quad \lambda = \sqrt{\frac{\alpha^*}{2\pi q}} \qquad (3.15)$$

u_ϕ , e and ω are now given by (3.8). Fig. 3.2 shows the circulation distribution so obtained. It will be observed that at first Γ increases as η increases from zero and overshoots Γ_0 by about 40% before it decreases to Γ_0 as η approaches λ. The presence of this overshoot can easily be demonstrated from (3.12). Substitution of (3.12) in (3.11) shows that $A_1 = -2$ and thus from (3.13)

$$\Gamma = \Gamma_0 \bar{F} \bar{\eta}$$

$$\sim \Gamma_0 (1 - 2\xi \ell n \xi)(1-\xi)$$

Thus for small ξ, $\Gamma > \Gamma_0$. This behavior is in accordance with the structure of solutions of the model equations near a turbulent-non-turbulent interface already discussed in the previous chapter.

We now proceed to evaluate u_z and p from the first two of (3.7). By defining $P(\eta)$ by the equation

$$p = \frac{\rho U \Gamma_0}{z} P(\eta) \tag{3.16}$$

we have the equation for $P(\eta)$ from (3.7) as:

$$\frac{dP}{d\eta} = \frac{F^2}{\eta} \tag{3.17}$$

We can, without loss of generality, take the pressure at infinity to be zero. Since circulation for $\eta > \eta_0$ is constant and equal to Γ_0, we can integrate (3.17) for $\eta > \lambda$ and find that

$$P(\lambda) = - \frac{A_0^2}{2} . \tag{3.18}$$

$P(\eta)$, for $\eta < \lambda$, can be found by numerically integrating (3.17) using the boundary condition (3.18). The numerical integration is best performed in the new variable, $\bar{P}(\bar{\eta}) = P(\eta)/A_0^2$, in terms of which (3.17) and (3.18) become

$$\frac{d\bar{P}(\bar{\eta})}{d\bar{\eta}} = \frac{\bar{F}^2}{\bar{\eta}} ; \qquad \bar{P}(1) = -\tfrac{1}{2} . \tag{3.19}$$

We can now determine u_z starting from (3.7). We write the equation for u_z in the independent variables η, z, thus:

$$\frac{\partial u_z}{\partial z} - \tfrac{1}{2}\frac{\eta}{z}\frac{\partial u_z}{\partial \eta} - \frac{1}{z\eta}\frac{\partial}{\partial \eta}\left(\frac{J}{K}\eta\frac{\partial u_z}{\partial z}\right) = \frac{\Gamma_0}{z^2}\frac{1}{2\eta}\frac{\partial}{\partial \eta}(P\eta^2) \tag{3.20}$$

Equation (3.20) is a linear diffusion equation for u_z. Batchelor (1964) studied the properties of a similar equation in connection with axial flow in a laminar trailing vortex. A study of his solution indicates that the above equation has an asymptotic solution, valid for large z, of the form

$$u_z = U - \frac{\Gamma_0}{z}\ln\frac{Uz}{\Gamma_0}\cdot Q_1(\eta) + \frac{\Gamma_0}{z}\cdot Q_2(\eta) \tag{3.21}$$

Ordinary differential equations for Q_1 and Q_2 are obtained by using (3.21) in (3.20) and equating terms of equal powers in z. They are:

$$Q_1 + \frac{\eta}{2}Q_1' + \frac{1}{\eta}\frac{d}{d\eta}\left(\frac{J}{K}\eta\frac{dQ_1}{d\eta}\right) = 0$$

$$Q_2 + \frac{\eta}{2}Q_2' + \frac{1}{\eta}\frac{d}{d\eta}\left(\frac{J}{K}\eta\frac{dQ_2}{d\eta}\right) = -\frac{1}{2\eta}(P\eta^2) - Q_1 \tag{3.22}$$

As $u_z - U = 0$ for $\eta \geq \lambda$, we have $Q_1(\lambda) = Q_2(\lambda) = 0$. Also, Q_1 and Q_2 must be bounded as $\eta \to 0$. These conditions along with (3.22) are sufficient to determine Q_1 and Q_2. We integrate the equation for

Q_1 once and choose the constant of integration so that $Q_1(\lambda) = 0$ to get

$$\frac{dQ_1}{d\eta} = - \frac{\eta K}{2J} Q_1 \tag{3.23}$$

(3.23) is a linear equation for Q_1. A numerical integration determines Q_1 but for an arbitrary constant factor.

We perform an integration of the equation for Q_2 and choose the constant of integration such that Q_2 is nonsingular at $\eta = 0$ to get

$$\frac{Q_2 \eta^2}{2} + \frac{J}{K} \eta \frac{dQ_2}{d\eta} = - \frac{P \eta^2}{2} - \int_0^\eta Q_1 \eta \, d\eta \tag{3.24}$$

The left hand side of (3.24) tends to zero as η tends to zero for nonsingular Q_2. Thus the right hand side must also be zero and the choice of the arbitrary constant satisfies this requirement. Also we have $Q_2(\lambda) = 0$. As $\frac{J}{K} = 0$ at $\eta = \lambda$, we have from (3.24)

$$- \frac{P(\lambda) \lambda^2}{2} - \int_0^\lambda Q_1 \eta \, d\eta = 0 \tag{3.25}$$

Equation (3.25) determines the arbitrary constant factor in Q_1. Equation (3.24) can then be integrated to get Q_2. (3.24) is a linear first order equation and its solution contains the complimentary function with an undetermined coefficient. This function includes any wake which may be present due to an initial momentum defect. However, for the sake of definiteness, we can choose the constant so that $Q_2(0) = 0$. We can then add any u_z distribution corresponding

to the initial defect of momentum separately. This wake profile has the same form as Q_1 but decays as $1/z$. As u_z associated with Q_1 decays more slowly (as $\log z/z$), for sufficiently large z, it dominates the u_z associated with Q_2 or any initial momentum defect.

For convenience in numerical work we define

$$Q_1(\eta) = A_0^2 \bar{Q}_1(\bar{\eta})$$

$$Q_2(\eta) = A_0^2 \bar{Q}_2(\bar{\eta}) \tag{3.26}$$

to get

$$\frac{d\bar{Q}_1}{d\bar{\eta}} = -\frac{\bar{\eta}}{2}\frac{\bar{K}}{\bar{J}}\bar{Q}_1$$

$$\frac{\bar{J}}{\bar{K}}\bar{\eta}\frac{d\bar{Q}_2}{d\bar{\eta}} + \frac{\bar{Q}_2\bar{\eta}^2}{2} = -\frac{\bar{P}\bar{\eta}^2}{2} - \int_0^{\bar{\eta}} \bar{Q}_1\bar{\eta}\, d\bar{\eta}$$

$$\int_0^1 \bar{Q}_1\bar{\eta}\, d\bar{\eta} = \tfrac{1}{4} \tag{3.27}$$

Some results obtained by numerical integration are shown in Fig. 3.3.

3.3 Discussion.

The circulation profile corresponding to the present analysis is compared with the profile derived from various sources in Fig. 3.2. McCormick's profile was derived from the vortimeter data already mentioned. Rose and Dee's measurement of maximum velocity in

a vortex locates a single point in the profile. The profile shown in the figure was obtained by assuming that it follows the logarithmic form of Hoffman and Joubert and using a $\Gamma_1/\Gamma_0 = 0.37$ and a Γ_0 one half its value at the wing root corresponding to McCormick's data. The profile for constant eddy viscosity was derived from equation (3.4) with a chosen to be 2×10^{-4} roughly in agreement with the value quoted by Rose and Dee. For any other a, the profile is laterally shifted, but unaltered in shape. We immediately notice considerable differences among the various profiles.

Rose and Dee's data imply a radius of the vortex (defined as the radius at which circulation reaches 95% of its value at infinity) roughly twice that of McCormick's. The present analysis yields a radius for the sharp turbulent-nonturbulent interface roughly three times the radius of the vortex as estimated from the data of Rose and Dee. But the present solution has another radius at which circulation is equal to its value at the interface and beyond. If we compare the radius of the vortex corresponding to the smaller value, the disagreement is much reduced.

We also note the flatness of McCormick's profile as compared with the present solution or that for constant eddy viscosity. Further, the model equations predict a circulation profile with an overshoot of about 40% above the circulation at infinity. Experiments do not indicate the presence of any significant overshoot. Thus the circulation profile as derived from model equations is not satisfactory in this respect. Also, we know (Rayleigh 1916) that inviscid vortex flows with circulation decreasing with radius are unstable. This

strongly suggests instability of the present solution.

It is obvious from the above, that the model equations, as they are, do not explain the growth of a vortex sufficiently well. The most significant shortcoming is the indication of a large overshoot in the circulation profile. It is possible to remedy the situation by modifying the model equations. Evidently, it is most convenient to make such modifications as will leave the results obtained in Chapter 2 unaltered. Since vortex flow is the only one, so far, with streamline curvature, addition of terms in the model equations depending on it are satisfactory in this respect. One such possibility, suggested by Saffman, is to include a term $c\sqrt{J}\,\frac{d\Gamma^2}{d\eta}$ in the last of (3.9). It will be seen that the new term has the right dimensions and still permits a sharp interface. Also, near a turbulent-nonturbulent interface J is small so that $\sqrt{J}$ dominates J and thus the additional term is likely to modify the solution near an interface considerably. It looks possible to choose the constant c in the additional term so that the overshoot in the circulation profile is eliminated or at least very much reduced. The feasibility of this scheme is still unverified.

Now, some comments about the experimental studies of the trailing vortices are in order. As the Table 3.1 indicates, wind tunnel studies of the vortices are for a Reynolds number (i.e. $\frac{\Gamma_0}{\nu}$) in the range $10^3 - 10^5$ while the flight tests are for a Reynolds number in the range $10^6 - 10^7$. From the table it is seen that the vortex growth rate as indicated by a in the table is significantly different for the flight tests and the wind tunnel experiments. This

difference, barring experimental errors, can only be attributed to the effect of Reynolds number. It is interesting to note here that the vortex growth rate indicated by the analysis using model equations roughly agrees with the wind tunnel data at the highest obtained Reynolds number.

The data about vortex growth at the higher Reynolds numbers come from the only two flight studies to date. The flight studies are difficult and the accuracy of this data is not known. Wind tunnel studies available do not cover the range of Reynolds numbers $10^5 - 10^7$. It looks desirable to conduct accurate studies of the vortex at these Reynolds numbers in a wind tunnel.

Such a study of the trailing vortex in a wind tunnel can be conveniently carried out using a wing spanning the test section such that one half of the wing has an angle of attack equal and opposite to the other. The vortices from the two halves of the wing merge to form a single vortex from the centre of the wing. Based on experimental results already quoted, we may assume that the strength of the vortex is half the sum of the circulations of the two parts of the wing. From this we have an estimate for the vortex Reynolds number, $\frac{\Gamma_0}{\nu}$, and the radius of the vortex, r_0 (i.e. the radius at which circulation is $0.95\ \Gamma_0$) as:

$$\frac{\Gamma_0}{\nu} = \frac{C_L uc}{2\nu}$$

$$r_0 = k\sqrt{\frac{C_L c\, z}{2}} \qquad (3.28)$$

C_L is the lift coefficient of either half of the wing of chord c. k is a constant whose value from Rose and Dee's data is about 0.1. Wind tunnel data of Table 3.1 indicate a k of about 0.3. The axial distance z, in equation (3.28) is assumed large compared with the distance required for vortex formation. At the present time, no reliable data about the axial distance required for the roll up of the vortex sheet into the vortices and their approach to similarity form exist. McCormick (1968) found that, in his full scale experiments, the roll up was nearly complete in a distance of about one chord length behind the trailing edge of the wing. The dependence of this roll up distance on other dimensions of the wing and the free stream velocity is not known. In general, we expect the roll up process and the approach to similarity form to occupy an axial distance of a few chord lengths behind the wing. Thus it looks desirable to study the vortex in the range of at least 5 to 50 chord lengths downstream of the wing.

For studying the vortex at a Reynolds number of about 10^6, the above considerations indicate a wing of chord about 2.5 feet in a stream of 100 feet per second. The radius of the vortex so formed is about 1 foot at 10 chords (25 feet) behind the wing. Some wind tunnels in existence have test sections big enough to generate a vortex of this size. But these test sections are not long enough for a study extending to 50 chord lengths (125 feet) downstream of the wing. It looks feasible to study a vortex at a Reynolds number of 10^5 which can be produced by a wing of chord 6 inches in a stream of 50 feet per second. This vortex has a diameter of about 6 inches

at an axial distance of 50 chords (25 feet). Even this study is likely to provide valuable data about the trailing vortices.

3.4 Concluding Remarks.

It is clear that the model equations have some shortcomings which are to be eliminated before we have a reliable method for treating turbulent flows. The shortcomings can only be eliminated by the trial and error procedure of modifying the equations so that solutions obtained using the model agree with experiments in a variety of flow situations. This procedure is expensive in terms of time and effort because of the complexity of the equations. Thus much work needs to be done before we can meet the demand for a method capable of application to novel situations without the aid of experiments.

Appendix I.

We can obtain a structure for the interface considered in Section 1.4 by formally introducing an index of viscosity, ν, into equations (1.12). For simplicity we retain only the leading terms of (1.12) and we have

$$\frac{\partial v}{\partial t} + u \frac{\partial v}{\partial x} = \frac{\partial}{\partial x}\left[\left(\frac{e}{\omega} + \nu\right) \frac{\partial v}{\partial x}\right]$$

$$u \frac{\partial e}{\partial x} = \frac{\partial}{\partial x}\left[\left(\frac{e}{2\omega} + \nu\right) \frac{\partial e}{\partial x}\right]$$

$$u \frac{\partial \omega^2}{\partial x} = \frac{\partial}{\partial x}\left[\left(\frac{e}{2\omega} + \nu\right) \frac{\partial \omega^2}{\partial x}\right] \qquad \text{(A.1)}$$

For analytical convenience we restrict our attention to a similarity type of solution of (A.1) which has the form

$$v = F(x)e^{\alpha t} \; ; \; e = J(x)\, e^{\alpha t} ; \; \omega = K(x)\, e^{\alpha t} \qquad \text{(A.2)}$$

where α is a real constant. Then (A.1) implies

$$\alpha F + u \frac{dF}{dx} = \frac{d}{dx}\left[\left(\frac{e}{\omega} + \nu\right) \frac{dF}{dx}\right]$$

$$u \frac{dK^2}{dx} = \frac{d}{dx}\left[\left(\frac{e}{2\omega} + \nu\right) \frac{dK^2}{dx}\right]$$

$$u \frac{dJ}{dx} = \frac{d}{dx}\left[\left(\frac{e}{2\omega} + \nu\right) \frac{dJ}{dx}\right] \qquad \text{(A.3)}$$

The interface conditions of Section 1.4 imply that as $\nu \to 0$

$$F = v_0 \; ; \quad J = 0 \quad ; \quad K = 0 \qquad \text{for} \quad x < 0$$

$$F = a_0 + a_1 x \ell n x + a_2 x + o(x) \; ; \; J = b_0 x^2 \; ; \; K = \frac{b_0 x}{u} \text{ for } x > 0 \qquad (A.4)$$

with $a_0 = \frac{u a_1}{\alpha}$. b_0 and a_2 are arbitrary constants.

For small ν, not equal to zero, we can consider (A.4) as the outer solution of (A.3). The inner equations are easily obtained by introducing the scaled variables

$$F(x) = \overline{F}(\overline{x}), \; J(x) = \nu^2 \overline{J}(\overline{x}), \; K(x) = \nu \overline{K}; \; x = \frac{\overline{x}\nu}{u} \qquad (A.5)$$

(A.3) in the scaled variables, with $\overline{E} = \overline{J}/\overline{K}$, are

$$\frac{d}{d\overline{x}}\left[(\overline{E}+1)\frac{d\overline{F}}{d\overline{x}}\right] = \frac{\nu\alpha}{u^2}\overline{F} + \frac{d\overline{F}}{d\overline{x}}$$

$$\frac{d\overline{J}}{d\overline{x}} = \frac{d}{d\overline{x}}\left[(\frac{\overline{E}}{2}+1)\frac{d\overline{J}}{d\overline{x}}\right]$$

$$\frac{d\overline{K^2}}{d\overline{x}} = \frac{d}{d\overline{x}}\left[(\frac{\overline{E}}{2}+1)\frac{d\overline{K^2}}{d\overline{x}}\right] \qquad (A.6)$$

The solutions for $\overline{J}$ and $\overline{K}$ satisfying (A.4), which gives

$$\overline{J} \to 0 \; , \; \overline{K} \to 0 \quad \text{as} \quad \overline{x} \to -\infty$$

$$\overline{J} \to \frac{b_0}{u^2}\overline{x}^2 \; , \; \overline{K} = \frac{b_0}{u^2}\overline{x} \quad \text{as} \quad \overline{x} \to +\infty \qquad (A.7)$$

are implicitly given by:

$$\overline{J} = \frac{u^2}{b_0}\,\overline{K}$$

$$2\log\frac{\overline{K}u^2}{b_0} + \frac{u^2\overline{K}}{b_0} = \overline{x} \tag{A.8}$$

(A.4) implies an $\overline{F}$ of the form

$$\overline{F}(\overline{x}) = a_0 + \nu\,\ell n\nu\, F_1(\overline{x}) + \nu F_2(\overline{x}) + o(\nu) \tag{A.9}$$

Using (A.9) in the first of (A.6) we have equations for F_1 and F_2 as

$$\frac{d}{dx}\left[(\overline{E}+1)\frac{dF_1}{dx}\right] = \frac{dF_1}{dx}$$

$$\frac{d}{dx}\left[(\overline{E}+1)\frac{dF_2}{dx}\right] = \frac{a_0\alpha}{u^2} + \frac{dF_2}{dx} \tag{A.10}$$

Boundary conditions for F_1 and F_2 are obtained from (A.4) as

$$F_1 \to 0, \quad F_2 \to 0 \quad \text{as} \quad \overline{x} \to -\infty$$

$$F_1 \to \frac{a_1\overline{x}}{u}, \quad F_2 \to \frac{a_1\overline{x}}{u}\left(\ell n\frac{\overline{x}}{u} + \frac{a_2}{a_1}\right) \tag{A.11}$$

We can easily obtain F_1 to satisfy (A.11) in an implicit form as:

$$F_1 = \frac{a_1 u^3}{b_0^2}\,\frac{\overline{K}^2}{\left(1 + \frac{u}{b_0}\overline{K}\right)^2} \tag{A.12}$$

Solution for F_2 is easily obtained by the method of variation of parameters and is

$$F_2 = F_1 \left[\frac{a_2}{a_1} + \frac{a_0 \alpha}{u^2} \int_{-\infty}^{\bar{x}} \frac{y \, dy}{\{ \bar{E}(\eta) + 1 \} F_1(\eta)} \right] \qquad (A.13)$$

The integral in (A.13) behaves like $\log \bar{x}$ for large $\bar{x}$ and thus satisfies (A.11).

Saffman (1969) considered the problem of a turbulent front with viscosity moving into stagnent fluid. This corresponds to the present solution with $\alpha = 0$. Thus the above analysis can be considered a generalization of Saffman's solution.

REFERENCES - Part II

1. Batchelor, G.K., (1964) Axial Flow in Trailing Vortices, J. F. M., Vol. 20, Part 4, pp.645-658.

2. Bradbury, L.J.S., (1965) The Structure of a Self-preserving Turbulent Plane Jet, J.F.M., Vol. 23, Part 1, pp. 31-64.

3. Dosanjh, D.S., Gasparek, E.P., and Eskinazi, S., (1962) The Decay of Viscous Trailing Vortices, Aero. Qtly., 13, p. 167.

4. Harlow, F.H., and Nakayama, P.I. (1967) Turbulence Transport Equations, Phys. Fluids, 10, p. 223.

5. Hinze, J.O., (1962) Turbulent Pipe Flow, Mechanique de la Turbulence, Editions. du. centre National de la Recherche Scientifique.

6. Hoffman, E.R., and Joubert, P.N., (1963) Turbulent Line Vortices, J.F.M., Vol.16, Part 3, pp. 395-411.

7. Kolmogorov, A.N., (1942) Equations of Turbulent Motion of an Incompressible Fluid, S.S.S.R. Seria Fizicheska VI, No.1-2, pp. 56-58.

8. Lamb, H. (1932) Hydrodynamics, 6th Ed., Cambridge University Press.

9. McCormick, B.W., Tangler, J.L., and Sherrieb, H.E., (1968) Structure of Trailing Vortices, J. of Aircraft, Vol.5, No.3, pp. 260-267.

10. Newman, B.G., (1959) Trailing Vortex, Aero. Qtly., 10, p.148.

References, Part II - Cont'd.

11. Owen, P.R., (1964) The Decay of a Turbulent Trailing Vortex, A.R.C. 25818.

12. Prandtl, L., and Wieghardt, K., (1945) Uber ein Neues Formelsystem fur Ausgebildete Turbulenz, Nach. Akad. Wiss. Grottingen. Math. P Phy., Vol.IIA, 6.

13. Rayleigh, Lord, (1916) On the Dynamics of Revolving Fluids, Proc. Roy. Soc. A, 93, p. 148.

14. Robertson, J.M., (1959) A Study of Turbulent Plane Couette Flow, T. and A.M. Report No. 141, Dept. of Theoretical and Applied Mechanics, University of Illinois.

15. Rose, R., and Dee, F.W., (1965) Aircraft Vortex Wakes and Their Effects on Aircraft, Aero. Res. Council, C.P. 795.

16. Saffman, P.G., (1969) A Model for Inhomogeneous Turbulent Flow, Prepared for the Proceedings of the Boeing Scientific Research Labs. Symposium on Turbulence, 23-27 June, 1969, Seattle, Washington.

17. Schlichting, H., (1968) Boundary Layer Theory, 6th Ed., New York: McGraw-Hill.

18. Spalding, D.B., (1969) The Prediction of Two-dimensional Steady Turbulent Elliptic Flows, Paper Presented at the 1969 Seminar on Heat and Mass Transfer in Flows with Separated Regions, Herieg Novi, Yugoslavia.

19. Squire, H.B., (1954) The Growth of a Vortex in Turbulent Flow, A.R.C. 16, 666.

References, Part II - Cont'd.

20. Townsend, A.A., (1956) The Structure of Turbulent Shear Flow, Cambridge University Press.

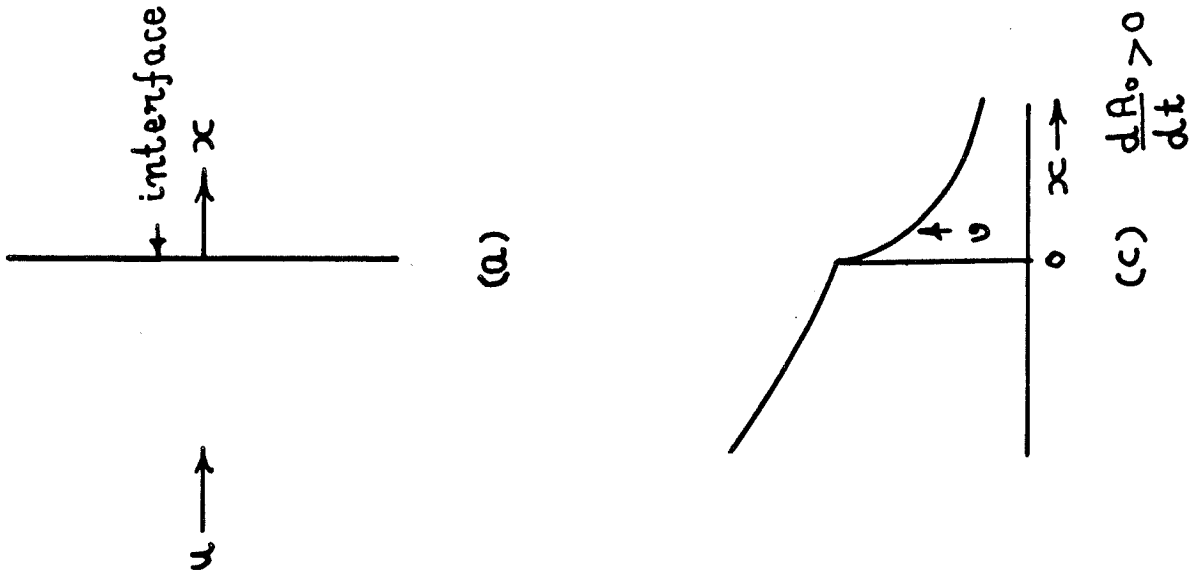
interface
x
y
(a)
v
x
0
(b) $\frac{dA_0}{dt} < 0$
v
x
0
(c) $\frac{dA_0}{dt} > 0$
v
x
0
(d) $\frac{dA_0}{dt} = 0$

FIG 1.1

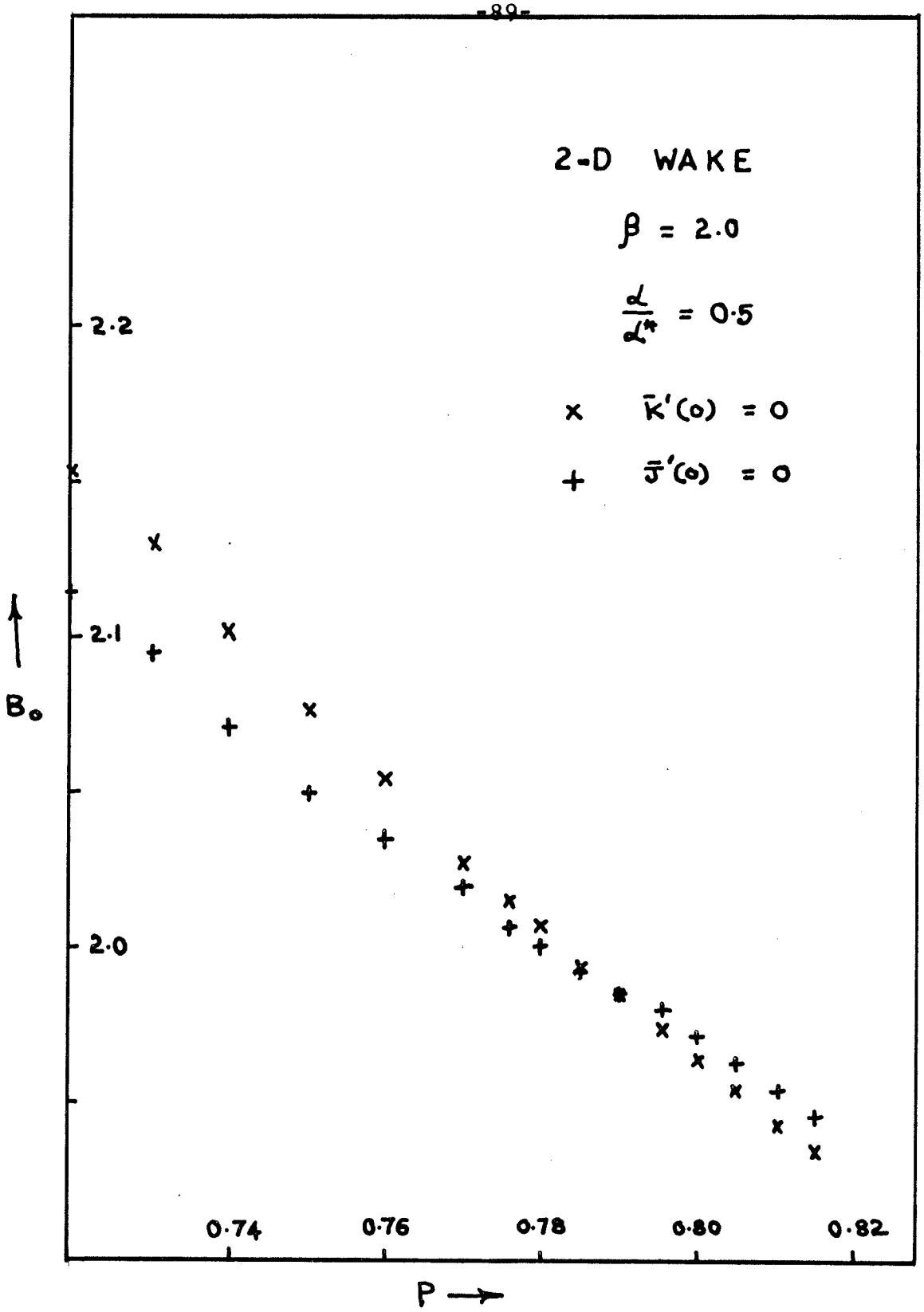

FIG 2.1

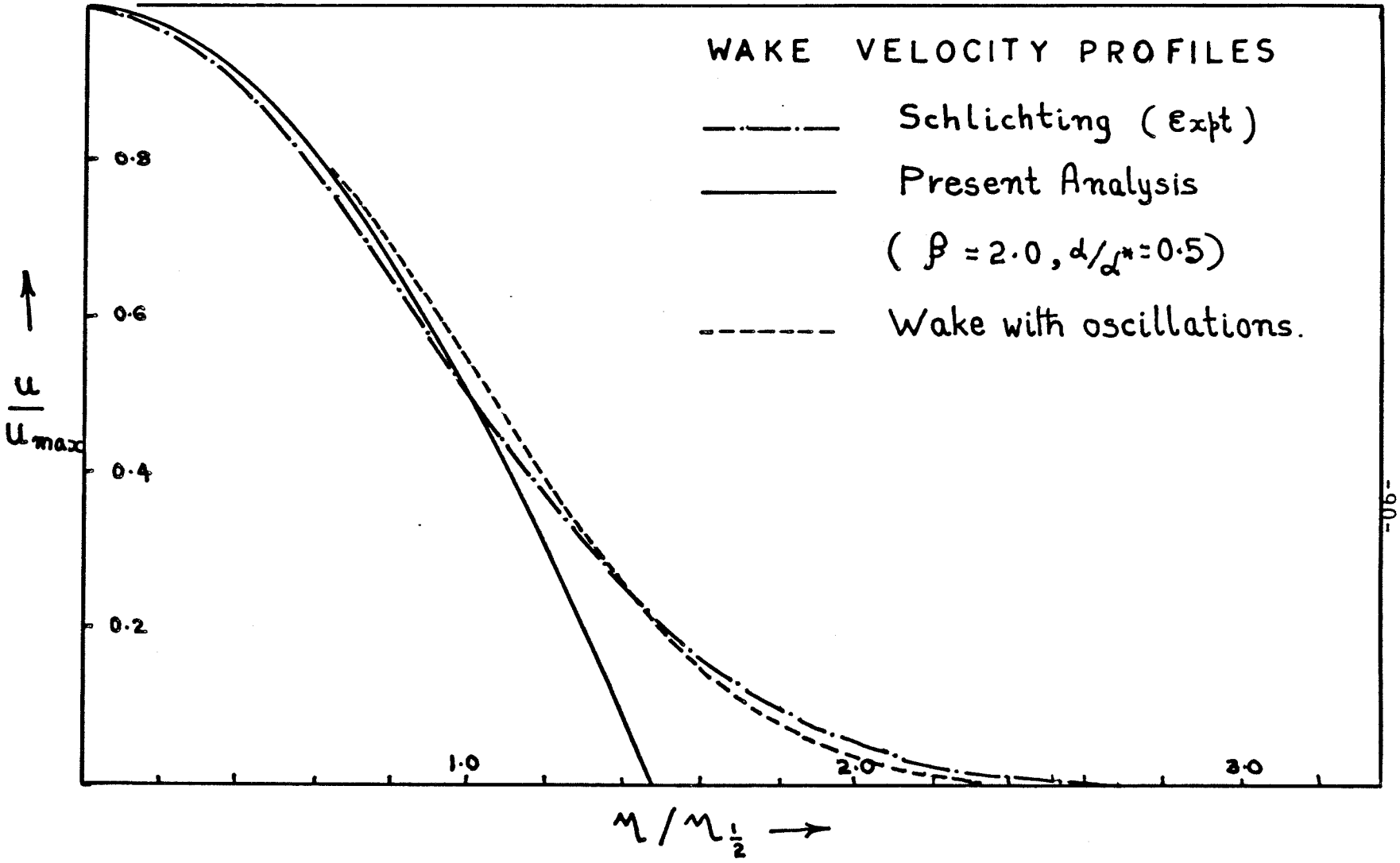
WAKE VELOCITY PROFILES
Schlichting (Expt)
Present Analysis
(β = 2·0, d/δ* = 0·5)
Wake with oscillations.
u / u_max
0·8
0·6
0·4
0·2
1·0
2·0
3·0
η / η_½

FIG 2.2

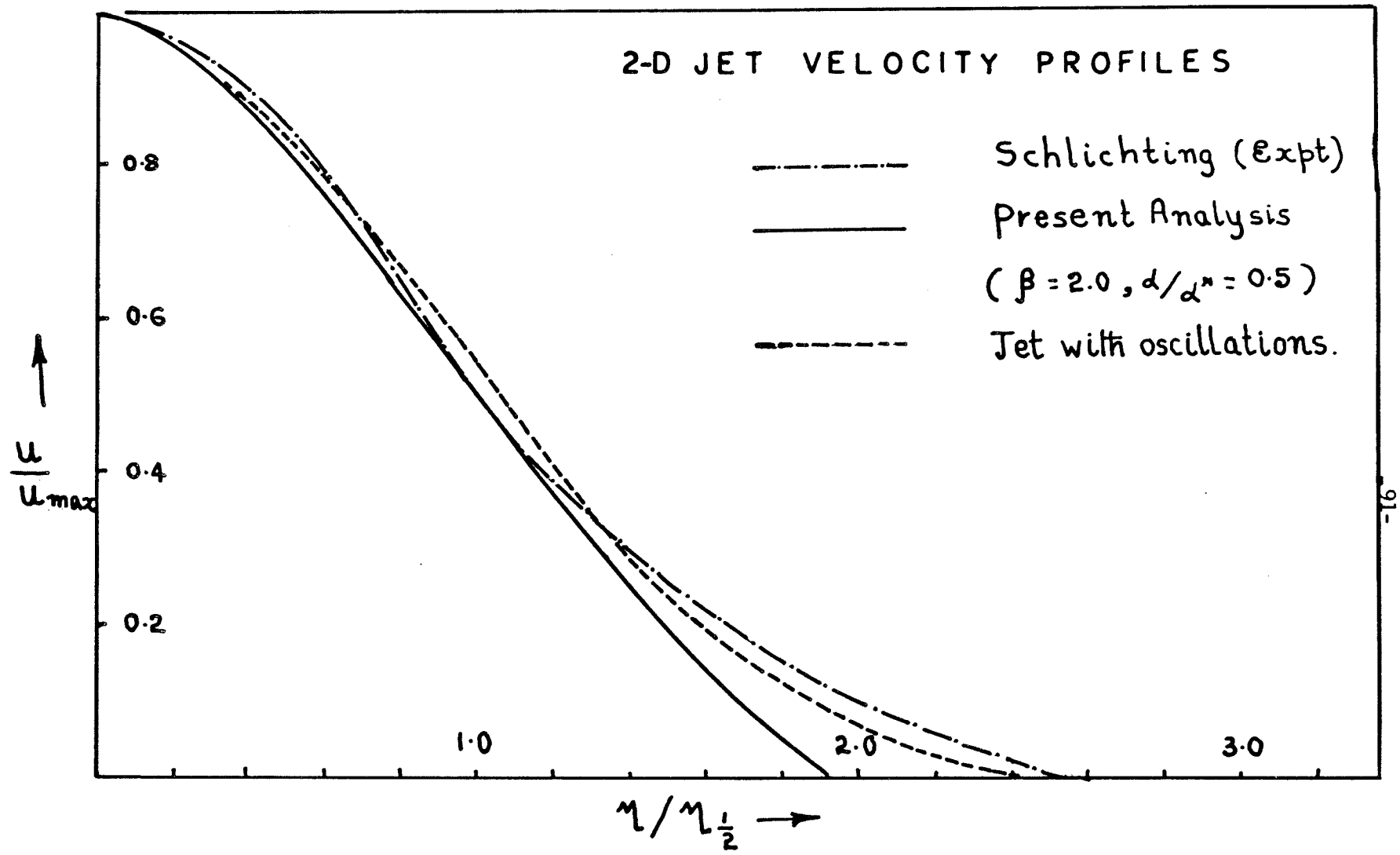
2-D JET VELOCITY PROFILES
Schlichting (Expt)
Present Analysis
(β = 2.0, d/d* = 0.5)
Jet with oscillations.
0·8
0·6
0·4
0·2
u/umax
1·0
2·0
3·0
η/η½

FIG. 2.3

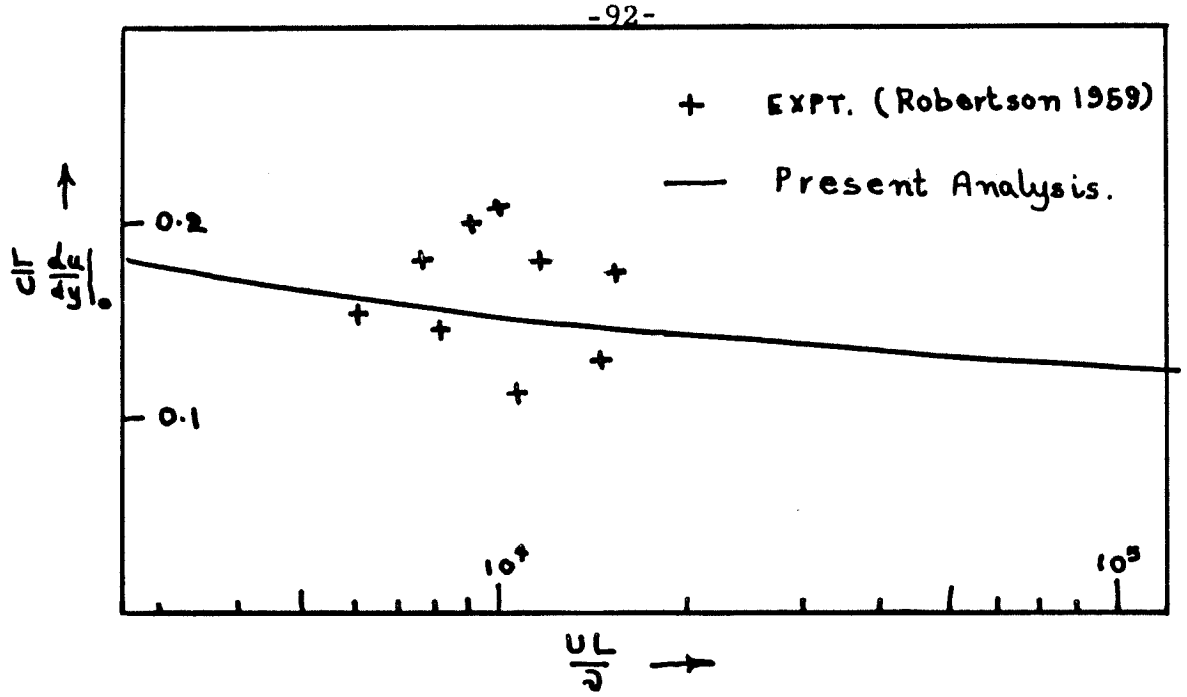
+ EXPT. (Robertson 1959)
Present Analysis.
0.2
0.1
$\frac{L}{U}\frac{du}{dy}\Big|_0$
10^4
10^5
$\frac{UL}{\nu}$

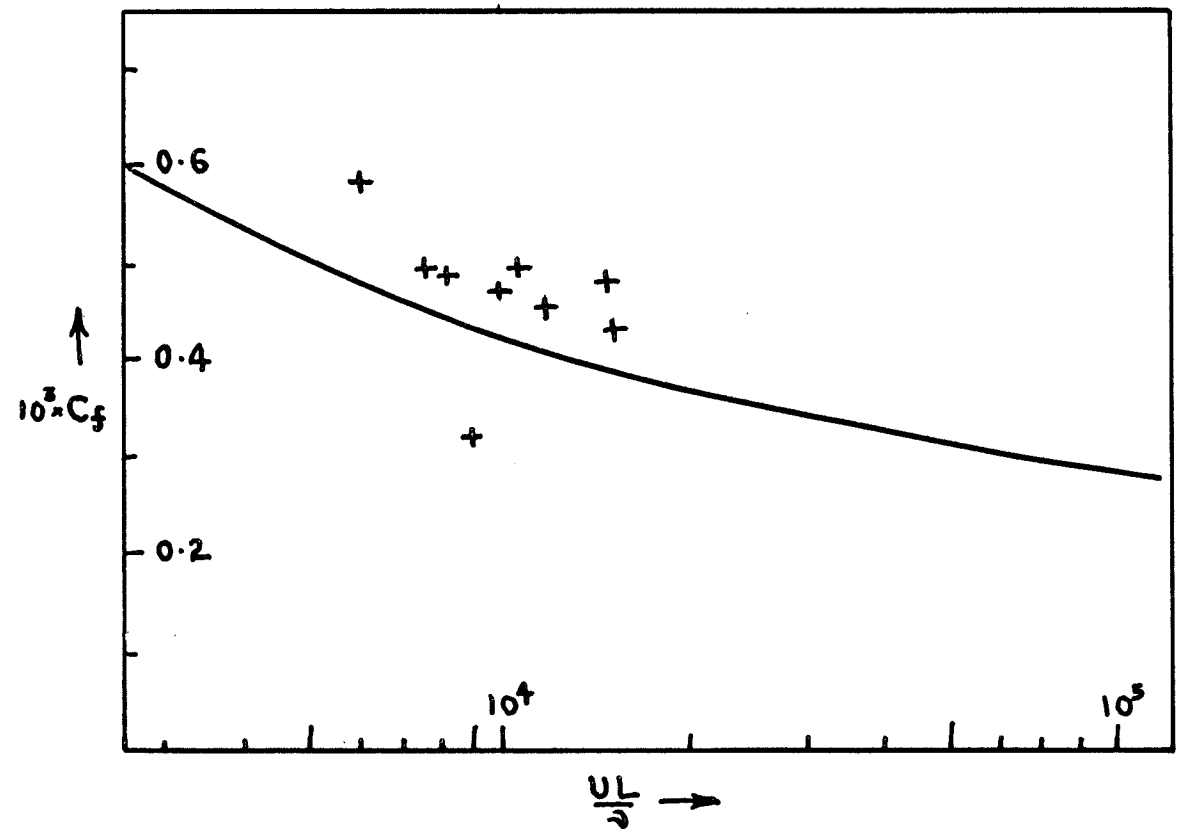
0.6
0.4
0.2
$10^3 \times C_f$
10^4
10^5
$\frac{UL}{\nu}$

FIG 2.4

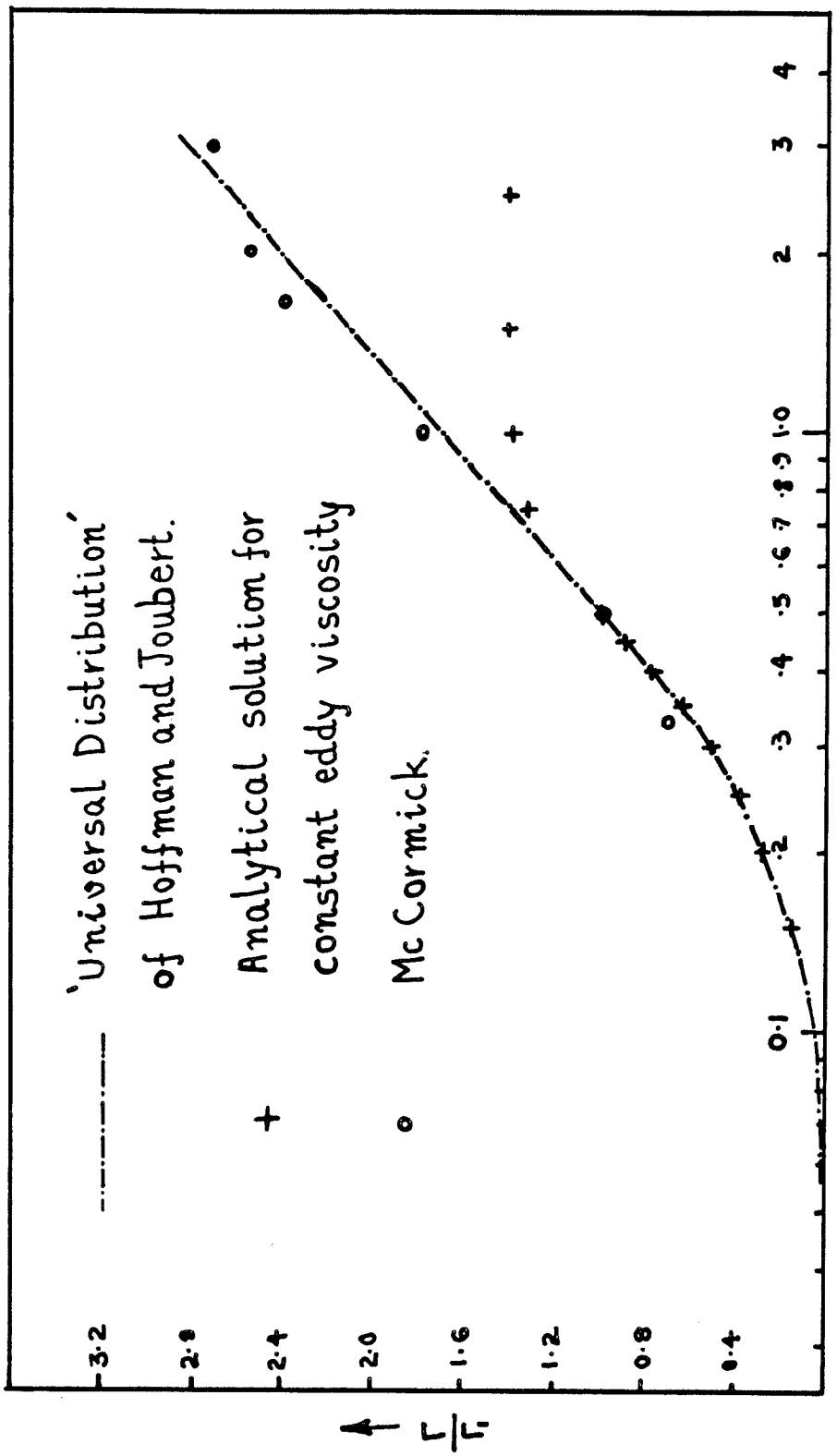

CIRCULATION DISTRIBUTION IN VORTICES

FIG 3.1

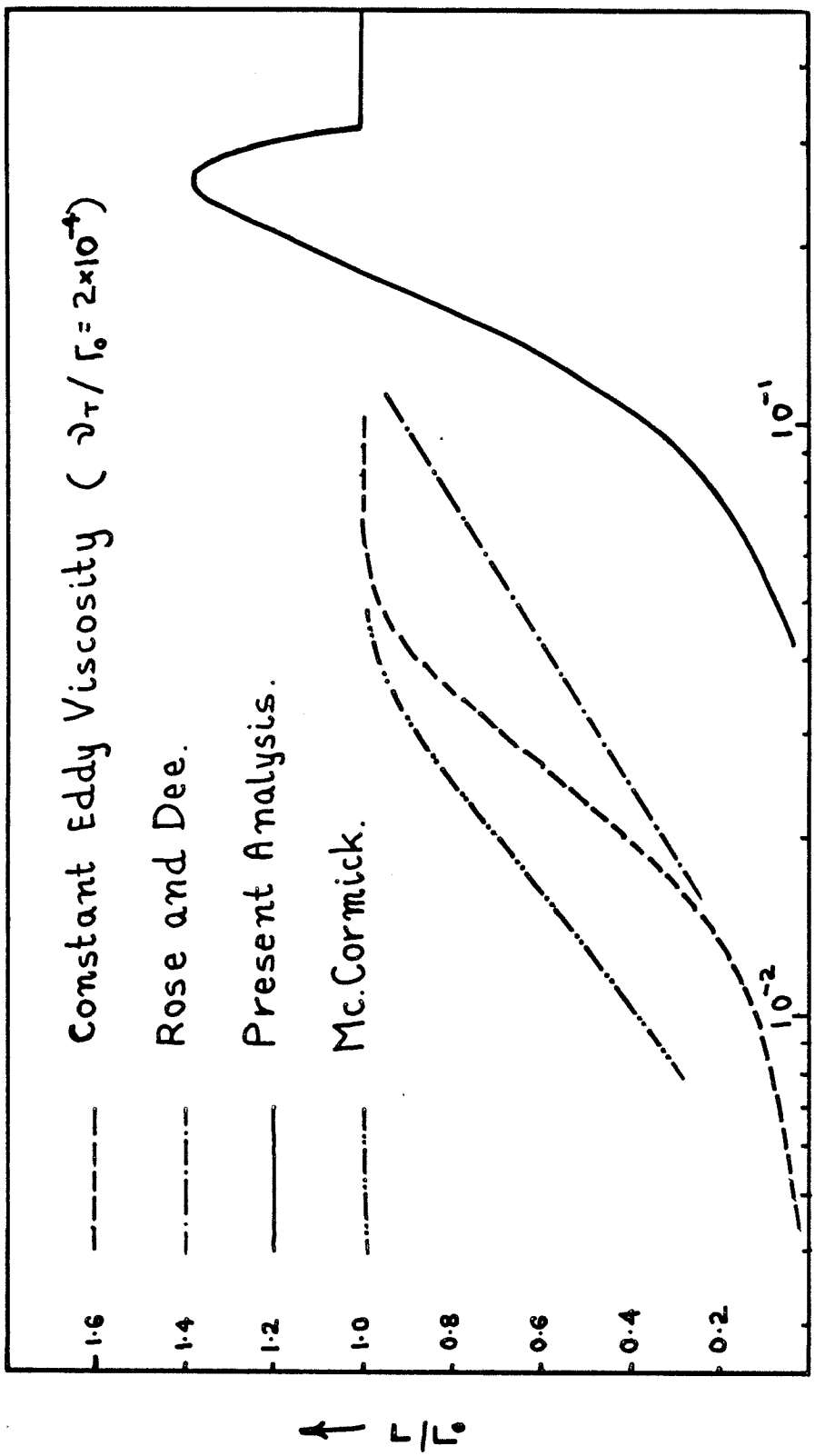

CIRCULATION DISTRIBUTION IN VORTICES

FIG 3.2

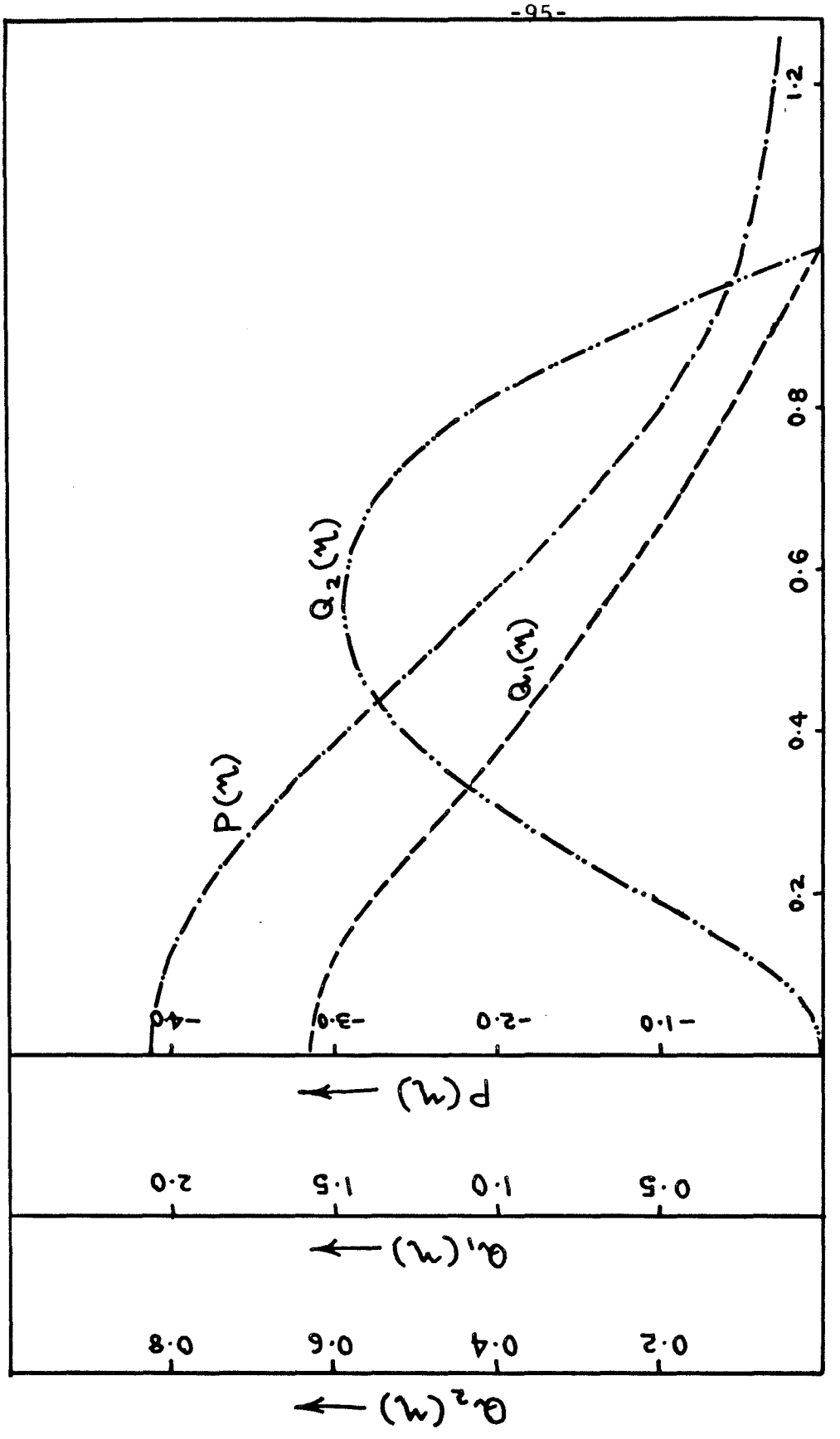
P(η)
Q₂(η)
Q₁(η)
η/λ
0.2
0.4
0.6
0.8
1.2
-1.0
-2.0
-3.0
-4.0
P(η)
0.5
1.0
1.5
2.0
Q₁(η)
0.2
0.4
0.6
0.8
Q₂(η)

FIG 3.3